To the Graduate Council:

I am submitting herewith a thesis written by Hassan Ahmad Wahab entitled "Comparison of Classical and Modern Control Design for a Radar Antenna Drive." I have examined the final copy of this thesis for form and content and recommend that it be accepted in partial fulfillment of the requirements for the degree of Master of Science, with a major in Electrical Engineering.

J M Bailey

J.M. Bailey, Major Professor

We have read this thesis
and recommend its acceptance:

H.T. Mathews

[illegible]

Accepted for the Council:

C W Minkel

Vice Provost
and Dean of The Graduate School

STATEMENT OF PERMISSION OF USE

In presenting this thesis in partial fulfillment of the requirements for a Master's degree at The University of Tennessee, Knoxville, I agree that the Library shall make it available to borrowers under rules of the Library. Brief quotations from this thesis are allowable without special permission, provided that accurate acknowledgement of the source is made.

Permission for extensive quotation from or reproduction of this thesis may be granted by my major professor, or in his absence, by the Head of Interlibrary Services when, in the opinion of either, the proposed use of the material is for scholarly purposes. Any copying or use of the material in this thesis for financial gain shall not be allowed without my written permission.

Signature Hassan Wahab

Date Aug. 1990

COMPARISON OF CLASSICAL AND MODERN CONTROL DESIGN FOR A RADAR ANTENNA DRIVE

A Thesis

Presented for the

Master of Science

Degree

The University of Tennessee, Knoxville

Hassan Ahmad Wahab

August 1990

ACKNOWLEDGEMENTS

First of all, I want to thank God, the most gracious and merciful, for giving me his blessings, patience, and help in getting through my education, especially on this thesis.

I wish to express my appreciation to Dr. J.M. Bailey for being the chairman of my advisory committee, and to Dr. F.W. Symonds and Dr. H.T. Mathews for acting as members of my advisory committee.

It is a pleasure to acknowledge the support of Mr. Rafic AlHariri and his foundation for their support during this educational endeavor.

Thanks to Ms. Cindi Blair for typing the manuscript, and thanks to Mr. Mohammad AlJazar for doing to graphical manuscript. Also, special thanks are given to Mr. Ali NourAldine for his simulation help.

Finally, this thesis is dedicated to my family, relatives and friends, especially to my parents, Mr. and Mrs. Ahmad and Kahdigeh Wahab, my brothers Gahleb, Mohammad, Hussein; to my sweet sister Fatmeh, and to my future wife and son Em Ali and Ali.

ABSTRACT

The objective of this thesis is a comparison of classical and modern control design for a radar antenna drive. This drive is a DC motor which is used in an automatic tracking system. This drive requires a position controller in order to insure the desired operating characteristics. The emphasis of this thesis topic is to perform an analysis and design of the physical drive control system by modeling it mathematically. The design of the control system will be carried out using the classical method and the modern method. Then, a comparison is done to see which method will perform better and how close each method comes to meeting the given specifications operating on both servomechanism mode and regulator mode.

TABLE OF CONTENTS

LIST OF FIGURES

CHAPTER I

INTRODUCTION

1.1. Thesis Topic

The topic of this thesis is a comparison of classical and modern control design for a radar antenna drive. This drive is used in an automatic tracking system, which automatically follows a moving target as the result of the reflected signals received from that target. This automatic tracking requires generation of an error signal that compares between the reference voltage and the reflected signal through a nutator system [1]. The error signal is amplified to drive the DC motor in order to rotate the antenna so that it keeps track of the moving target. Conical scan of the antenna beam is frequently employed as the means of generating the error signal. The antenna system initiates the automatic tracking by scanning the beam for an incoming reflected signal. Presence of a target within the cone of acquisition will generate an error signal that enables the antenna system to position on the target and automatically track the target movement. Therefore, this requires a position controller for the DC machine drive in order to insure the desired operating characteristics. The emphasis of this thesis topic is to design classical and modern controllers for this system and compare them. Since this is a type 1 system with velocity input, the velocity constant K_V is an important parameter and its value is determined from the accuracy of the system.

1.2. Control Systems

In general, the objective of the control system is to control the outputs in some prescribed manner by the inputs through the elements of the control system.

There are two types of control systems:

1) Open-Loop Control Systems, which do not have a feedback and would not satisfactorily fulfill the desired performance requirements.

2) Closed-Loop Control Systems, which have a feedback. To obtain more accurate control, the controlled signal should be fed back and compared with the reference input, and an error signal proportional to the difference of the input and the output must be sent through the system to correct the error. Besides the reduction of error between the reference input and the system output, the feedback also has effect on such system performance characteristics as stability, bandwidth, overall gain, impedance, and sensitivity. There is positive feedback and negative feedback. The latter is used more widely and is the basis of the radar antenna drive control system, the topic of this thesis.

1.3. Analysis and Design of the Physical System

A schematic diagram of the control system is shown in Figure 1.1.

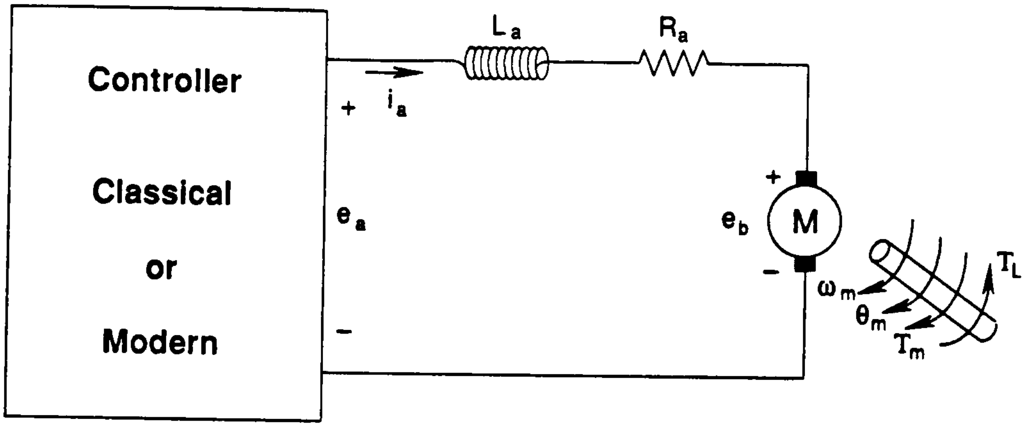

Figure 1.1

Schematic diagram for the control system

The machine used to drive the radar antenna is separately excited DC motor. The analysis and design of the control system is divided into the following steps. The first step is to find a mathematical description and model of the motor that is to be controlled. This step is one of the most important steps in the analysis and design of a control system, especially if the controller is going to be designed in an analytical way. For the given controlled motor, there is a set of variables that identify the dynamic characteristics of the motor which should first be defined, such as applied voltage, current in the motor armature windings, torque developed, angular velocity and angular displacement of the motor shaft, as the system variables. These variables are interrelated through physical laws that lead to algebraic and differential equations. In reality, some of these equations may be nonlinear. In order to establish practical analysis and design techniques, assumptions and approximations are going to be made to linearize the nonlinear equations. To complete this mathematical model, the system is portrayed by a block diagram and a signal flow graph. This is done by taking the Laplace transform of the motor differential equations and then finding the transfer function of the system. Also, by selecting the state variables of the motor, the state equation is found from the motor differential equations.

The second step is to find the physical parameters of the modeled motor, which are not provided. This is done experimentally by testing the DC motor. Third, the desired specifications for the control system are set so that the unit step input transient performance is defined such as overshoot, delay time, rise time, and settling time. Fourth, an analytical study is done on the motor along with the controllers. This is done by:

1) After taking the Laplace transform of the motor differential equations and then finding the transfer function, a classical controller is analyzed for the system in order to meet the given specifications.

2) After setting the state variables of the motor, state space equation is found in the vector matrix form, $x^{\bullet} = Ax + Bu$.

Using the state equation, an optimal controller can be analyzed to meet the same given specifications.

In this system there are three state variables:

$i_a(t)$ = The armature current in amperes

$W(t)$ = The angular velocity in radian/sec

$\theta(t)$ = The angular displacement in radians

The control variable is $e_a(t)$.

The angular displacement, $\theta(t)$, is also the output controlled variable of the control system.

The control system has two modes of operations:

1) Servomechanism mode where T_L is zero and the desired output θ_d is the input.

2) Regulator mode where θ_d is zero and T_L is the input.

The system in actual operation will be in both of these modes. Since this system has been modeled as a linear system, the output would be the sum of the two modes of operation.

Fifth, a simulation of the control system is done with the different controllers after applying the wind disturbance which has been considered zero in the steps outlined above. This wind disturbance input represents a torque that the motor has to overcome in order to keep the antenna pointed at the target.

1.4. Conclusion

Finally, a comparison will be made between the classical controller and the modern controller working as servomechanisms to see how the controllers met the given specifications and which one performs better. Also, another comparison is given between the performance of these controllers with the system acting as a regulator. The control system is simulated by using the ACS, MATLAB, and other types of software.

CHAPTER II

MATHEMATICAL MODELING OF THE PHYSICAL SYSTEM

2.1. Introduction

One of the most important tasks in the analysis and design of control systems is the mathematical modeling of the systems.

The two most common methods are:

(a) The transfer function approach which is valid only for linear time-invariant systems;

(b) The approach of state equation which is first-order differential equation. This approach can be applied to portray linear as well as nonlinear systems.

In reality all physical systems are nonlinear to some extent. Therefore, in order to use transfer functions and linear state equations in the analysis and design of control system, the system must first be linearized or its range of operation must be limited or confined to a linear range.

Linearizing the system would decrease the complexity of the nonlinearity. Then, the task is to determine not only how to accurately describe the system mathematically but, more importantly, how to make proper assumptions and approximations whenever necessary, so that the system may be adequately characterized by a linear mathematical model.

2.2. DC Motors in Control Systems

Direct-current motors are one of the most widely used prime movers in the control systems.

This domination in today's industry is because DC motors are less difficult to control, especially for position control, and also AC motors characteristics are quite nonlinear, which makes the analytical task more difficult. On the other hand, DC motors are more expensive because of the brushes and commutators.

In today's technology, advanced manufacturing techniques have produced DC motors with ironless rotors and rotors with very low inertia, very high torque-to-inertia ratio, which have opened new applications for DC motors in computers as well as in the machine-tool industry [2].

The basic operational principle of a DC motor is a torque transducer that converts electric energy into mechanical energy. The torque developed on the motor shaft is directly proportional to the field flux and the armature windings current. Physically, the DC commutator machine consists of a rotating member called the armature, including commutator, located in the rotor, a stationary member which holds the field poles, located the stator, the air gap, and the yoke which is often an integral part of the machine housing (see Figure 2.1). Because of the commutator and brushes, the armature windings are located in the rotor and the field is located in the stator.

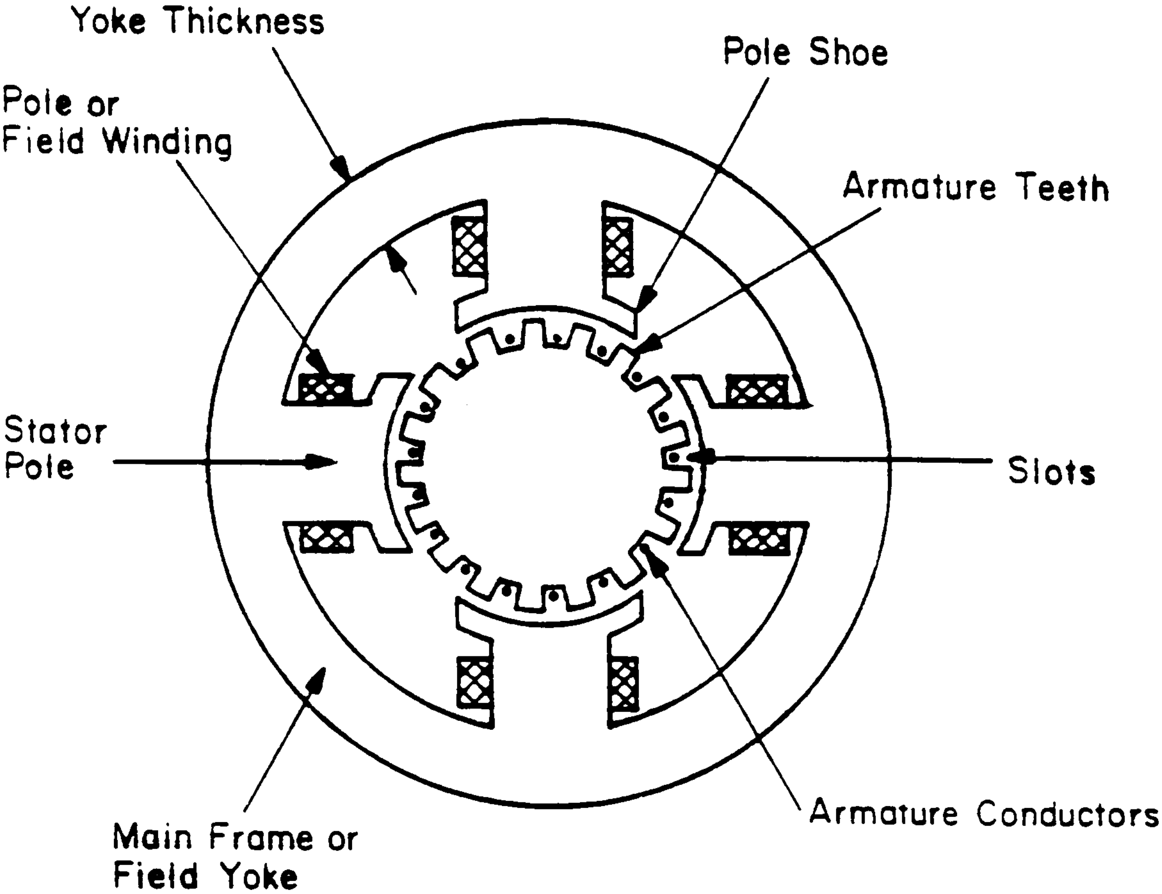

Figure 2.1

Cross section of a DC motor

There are two types of machine configurations:

(1) Radial air gap between the rotor and the stator, which is the most common. The rotating element is generally cylindrical in shape and fits inside the stator, which is a hollow cylinder or annular in shape and concentric with the rotor.

(2) Axial air gap which is not widely used.

The armature winding terminals are connected to the external power source through the commutator/brush system. This system acts as a mechanical switching device between the external armature circuit and the armature windings within the machine, in which currents and induced voltages are time-varying and reversing in polarity, so the polarity of the conductors in the armature windings are switched so a rotation will result. The external connections to the armature windings are made through the brushes resting on the commutator, which is held in stationary, fixed positions as the commutator and rotor turn. The rotor is mounted on a shaft that is supported on the bearings.

On the surface of the rotor there is a number of parallel, axial slots, in which are laid the armature coils that make up the armature windings.

There are two types of windings, lap and wave type.

(1) For lap winding: $\beta = mp$

(2) For wave winding: $\beta = 2$;

where

β = The number of parallel paths between armature winding terminals;

P = Number of magnetic field poles in stator;

M = Plex of the multiplex windings.

For a current-carrying conductor in the armature winding, immersed in a magnetic field with flux ϕ, and located at a distance r from the center of rotation, a torque will be developed. This torque is equal to:

$$T_m = k_T \cdot \phi \cdot i_a \tag{2.1}$$

where

T_m = Motor developed torque in Newton-meter;

ϕ = The net magnetic flux in the air gap in webers;

i_a = The armature current in ampers;

k_T = A proportional torque constant.

In addition to the torque developed, a voltage is generated across the terminal of the conductors in the armature windings due to the movement of these conductors in the magnetic field. This voltage, which is proportional to the shaft velocity and the magnetic field, tends to oppose the current flow. The relationship between this back emf and the shaft velocity is:

$$e_b = k_b \cdot \phi \cdot W_m \tag{2.2}$$

where

e_b = Back emf voltage in volts;

W_m = Shaft velocity of motor in radian/second;

k_b = A proportional, back emf constant.

Equations (2.1) and (2.2) are the basics of the DC motor operation that will be derived later. DC motors can be classified into several broad categories based on the way the magnetic field is produced and on the basic design and construction of the armature.

DC motors can be divided into three subclasses:

(1) Series-Field Motors, in which the field winding is connected in series with the armature. It has high torque at low speed.

(2) Shunt-Field Motors in which the field winding is parallel with the armature.

(3) Separately Excited Motors, in which the field winding is separated from the armature, which is the case considered in this control system topic. The magnetic flux is independent of the armature current, so this type of DC motor can be controlled externally over a wide range.

There are two basic winding configurations:

For Lap-Type Winding. The starting and terminating ends of adjacent coils overlap each others windings and are connected to adjacent commutator segments. The number of parallel paths is equal to the number of poles. This type of winding is used for low-voltage, high-current applications.

For Wave-Type Winding. The coils are connected in two parallel paths regardless of the number of poles. Most DC machines with ratings less than 75kw are constructed using this type of winding.

2.3. Derivation of Basic Equations of DC Machine [3]

The equations which relate the magnetic variables are:

$$\phi = B \cdot A$$

$$B = \mu \cdot H$$

$$H = \frac{F}{\ell}$$

$$R = \frac{\ell}{\mu \cdot A}$$

$$F = i(\ell \times B)$$

$$e_b = -\frac{d\phi}{dt} = -B\frac{dA}{dt} = BLU$$

where

A = Cross sectional area of armature coil conductor

ϕ = Magnetic flux in weber, Wb

B = Flux density in webers/meter^2 ; $(\frac{Wb}{m^2})$

F = mmf in ampere turns (aT)

R = Reluctance, no units

H = Field intensity in ampere turns/meter, (aT/m)

U = Linear velocity of the coil conductor in meters/second (m/sec)

μ = Permeability in Henry/meter (H/m)

i = current in armature coil conductor in Amperes (a)

ℓ = length of coil conductor in meters (m)

e_b = back emf , magnetomotive force, in volts (v)

These are used in the development of the basic equations of the DC motor:

a. Torque Equation. The operation of the DC motor is based on the tendency of a current-carrying coil, when placed in a magnetic field, to rotate in such a way that the field it creates is parallel to, and in the same direction as, the external field.

The general expression for the torque developed by a DC motor is derived as follows.

For the sake of simplicity, we derive the expression for torque by considering only a single-loop coil conductor in the armature winding. The instantaneous value of the torque developed (T_i) is determined by the partial derivative of the energy stored (W_f) in the armature winding, with respect to its angle of rotation (θ).

$$T_i = \frac{dw_f}{d\theta}$$

The incremental energy stored is given by:

$$dW_f = v_g \cdot i \cdot dt$$

where v_g is the voltage induced in a single turn of the armature current. From the above equations, we obtain

$$Ti = \frac{v_g \cdot i \cdot dt}{d\theta}.$$

Substituting for the voltage induced in terms of the flux linkage (λ), $v_g = \frac{d\lambda}{dt}$,

$$T_i = \frac{1}{\partial\theta}\left(i\,\frac{d\lambda}{dt}\,dt\right) = i\,\frac{d\lambda}{d\theta}\ .$$

As the motor turns dx of a revolution, the corresponding incremental change in the angle of rotation is $d\theta = 2\pi dx$ radians. Each side of the conductor cuts, only once, through the regions of the north and south magnetic field. That is, the incremental change of the flux linkage for each side of the single-turn armature winding is:

$$d\lambda = 2\phi(dx)\ .$$

The change in the flux linkage for the entire length of the winding is

$$d\lambda = 4\phi(dx) \quad \text{for a two-pole machine}$$

$$= 2P\phi(dx) \quad \text{for a P-pole machine}\ .$$

The current through the single winding is determined by the number of parallel paths of the armature winding and is related to the external armature current (i_a) by

$$i = \frac{i_a}{\beta}$$

From the above equations, the expression for the torque developed by a single conductor is:

$$T_i = \frac{P}{\beta T_i} \phi \cdot i_a \quad \text{N.m/turn} .$$

For N turns of the armature winding, the total torque developed (T_m) by the motor is:

$$T_m = \frac{N \cdot P}{\beta \cdot \pi} \phi \; i_a$$

or

$$T_m = k_T \cdot \phi \cdot i_a \quad \text{in (N.m)}$$

where the torque constant of proportionality K_T is given by:

$$k_T = \frac{NP}{\beta \pi}$$

Thus, the torque developed by a DC motor is directly proportional to the machines effective field, to the armature current, to the number of poles, and to the number of armature conductors.

b. Back emf Equation. The derivation of the second basic equation of the motor, $e_b = k_b \cdot \phi \cdot W_m$, is based on the induction principles, whereby the voltage is induced in a conductor that is rotated through an external magnetic field. The polarity of the induced voltage, by Lenzs Law, is in such a direction as to produce a current whose mmf opposes the external magnetic field. The conductor under consideration is the coil of the rotor.

The derivation of the general expression for the voltage induced is as follows.

The voltage induced in a single-turn armature winding is given by the time rate of change of the armature coil flux linkage.

$$v_g = \frac{d\lambda}{dt} ,$$

where v_g defined the voltage generated and λ defined the armature coils flux linkage. The change in the flux linkage of the armature winding that rotates through dx of a revolution is as before:

$$d_\lambda = 2P\phi \, dx \text{ for a P-pole machine.}$$

The increment of time that the winding requires to travel through dx of a revolution is:

$$dt = \frac{2\pi}{W_m}(dx) \text{ seconds,}$$

where W_m is the angular speed of the armature in radians/seconds. From the above equations,

$$v_g = \frac{P}{\pi} \phi \cdot W_m \quad \text{Volts/turn} .$$

The total voltage induced in the armature winding depends on the number of coil turns connected in series. From the last equation, the total voltage induced (e_b) in the armature conductors is:

$$e_b = \frac{NP}{\beta\pi} \phi \cdot W_m$$

or

$$e_b = k_b \cdot \phi \cdot W_m$$

Concerning the power in the motor, the electromagnetic power developed (P_d) by the machine is equal to the product of the electromagnetic torque developed (T_m) times the speed (W_m) of its rotor

$$P_d = T_m W_m \text{ Watts} .$$

Input electrical power = sum of various winding copper losses + power developed.

$$e_a \cdot I_a = I^2{}_f \cdot R_f + I^2{}_a \cdot R_a + P_d$$

where:

e_a and I_a = the motors supply (terminal) voltage and current.

$I^2{}_f \cdot Rf$ = the copper losses of the field winding.

$I^2{}_a \cdot Ra$ = the copper losses of the armature winding.

The power developed provides the output power (Pout) plus the rotational losses (P rot) ,

$$P_d = P\ rot + Pout\ .$$

To a certain extent rotational losses depend on the speed of the motor, but for linearization those losses are assumed to remain constant.

At nomial operating conditions, the output power is referred to as the rated power or the full-load power.

2.4. Dynamic Equations of the System

Having derived the basic equations they can be used for the mathematical modeling of the system.

The circuit diagram of the separately excited DC motor is shown again in Figure 2.2.

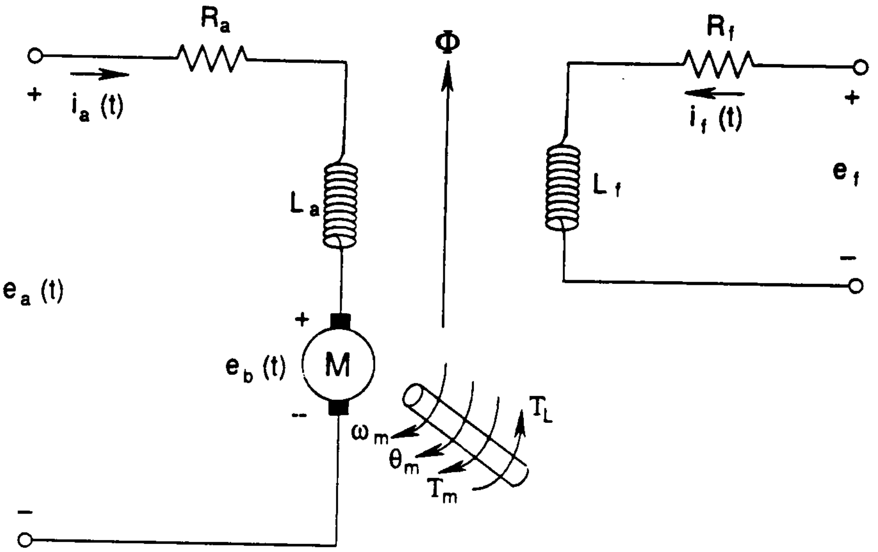

Figure 2.2

Model of a separately excited motor

The armature is modeled as a circuit with a resistance R_a in series with an inductance L_a , and a voltage source e_b representing the induced generated voltage (back mmf) in the armature when the rotor rotates. The field is represented by a resistance R_f in series with an inductance L_f . The air-gab flux is designated by ϕ .

The following summary on the variables and parameters is given:

$e_a(t)$ = Terminal voltage,	volt
$e_f(t)$ = Field voltage ,	volt
R_a = Armature resistence,	ohm
$e_b(t)$ = Back mmf,	volt
R_f = Field resistence,	ohm
L_a = Armature inductance,	Henry
L_f = Field inductance,	Henry
$i_a(t)$ = Armature current,	amp
$i_f(t)$ = Field current,	amp
K_T = Torque constant,	Newton meters/amp
K_b = Back mmf consant,	volts sec/rad
$\phi(t)$ = Net or air-gap magnetic flux,	Weber
$T_m(t)$ = Torque developed by motor,	Newton meter
J_m = Rotor inertia of motor,	kg meter^2
B_m = Viscous frictional coefficient,	Newton sec./meter
$\theta_m(t)$ = Rotor angular displacement,	Radian
$W_m(t)$ = Rotor angular velocity,	radians/sec
$T_L(t)$ = Disturbance torque,	Newton meter .

The units used for the above parameters are SI units.

J_m is the moment of inertia of the motor which includes the rotor and its shaft. The inertia is the property of an element that stores the kinetic energy of rotational motion. The inertia of a given element depends on the geometric composition about the axis of rotation and its density and it also represents the inherent property of bodies which resists any change in their state.

B_m is the viscous frictional coefficient of the motor which includes the rotor and its shaft. The viscous friction represents a retarding force that is approximated as a linear relationship between the applied torque and rotational velocity,

$$B = \frac{T_{rt}}{W_m} = \frac{P_{rt}/W_m}{W_m} = \frac{P_{rt}}{W_m^2}$$

With reference to the circuit diagram of Figure 2.2, the control is applied at the armature terminals in the form of the applied voltage $e_a(t)$, and $e_f(t)$ is assumed to have been applied sufficiently long so that the field current $i_f(t)$ is constant. For linear analysis, some assumptions are made further so that

1) The air-gap flux is proportional to the field current, that is,

$$\phi(t) = K_f \cdot I_f(t) = K_f \, I_f = \text{constant}.$$

2) The torque developed by the motor is proportional to the air-gap flux and the armature current. Thus,

$$T_m(t) = k_T \cdot \phi(t) \cdot i_a(t)$$

$$T_m(t) = k_T \cdot K_f \cdot I_f \cdot i_a(t)$$

$$T_m(t) = K_T \cdot i_a(t)\,, \qquad (2.3)$$

since

$$k_T \cdot K_f \cdot I_f = K_T = \text{constant}$$

where K_T is the torque constant. Also,

$$e_b(t) = k_b \cdot \phi(t) \cdot W_m(t)$$

$$e_b(t) = k_b \cdot K_f \cdot I_f\, W_m(t)$$

$$e_b(t) = K_b\, W_m(t) \qquad (2.4)$$

where K_b is the back emf constant.

a. State Equations

Starting with the control input voltage $e_a(t)$, the dynamic equations for the system are written:

$$e_a(t) = i_a \cdot R_a + L_a \frac{di_a(t)}{dt} + e_b(t)$$

$$\frac{di_{a(t)}}{dt} = \frac{1}{L_a} e_a(t) - \frac{R_a}{L_a} i_a(t) - \frac{1}{L_a} e_b(t)$$

$$\frac{di_{a(t)}}{dt} = \frac{1}{L_a} e_a(t) - \frac{R_a}{L_a} i_a(t) - \frac{K_b}{L_a} w_m(t) \qquad (2.5)$$

$$T_m(t) = T_L(t) + B_m \frac{d\,\theta_m(t)}{dt} + J_m \frac{d^2\,\theta_m(t)}{d+2} = K_T\, i_a(t)$$

$$\frac{d^2\,\theta_m(t)}{dt^2} = \frac{d\,W_m(t)}{dt} = \frac{1}{J_m} T_m(t) - \frac{1}{J_m} T_L(t) - \frac{B_m}{J_m} \frac{d\,\theta_m(t)}{dt} \qquad (2.6)$$

Since $\dfrac{d\,\theta_m(t)}{dt} = W_m$

$$dW_m(t)/dt = \frac{K_T}{J_m} i_a(t) - \frac{1}{J_m} T_L(t)\ \frac{B_m}{J_m} W_m(t) \qquad (2.7)$$

The state variables of the system are i_a, W_m, and θ_m. By direct substitution and elimination of all the nonstate variables from Equations 2.5 and 2.6, the state equations of the DC motor system are written in vector-matrix form:

$$\begin{bmatrix} di_a(t)/dt \\ dW_m(t)/dt \\ d\theta_m(t)/dt \end{bmatrix} = \begin{bmatrix} -R_a/L_a & -K_b/L_a & 0 \\ K_T/J_m & -B_m/J_m & 0 \\ 0 & 1 & 0 \end{bmatrix} \begin{bmatrix} i_a(t) \\ W_m(t) \\ \theta_m(t) \end{bmatrix} + \begin{bmatrix} 1/L_a \\ 0 \\ 0 \end{bmatrix} e_a(t) - \begin{bmatrix} 0 \\ 1/J_m \\ 0 \end{bmatrix} T_L(t) \qquad (2.8)$$

$$\theta_m(t) = [0 \quad 0 \quad 1] \begin{bmatrix} i_a(t) \\ W_m(t) \\ \theta_m(t) \end{bmatrix} \tag{2.9}$$

Notice that in this case $T_L(t)$ is treated as a second input in the state equations. But in the project case, this load input will be disregarded initially and will be used as disturbance input torque to simulate the system. The state diagram of the system is drawn as shown in Figure 2.3, where $T_L(t)$ denotes an additional load which represents a torque that the motor has to overcome in order to hold the output positions at a constant value.

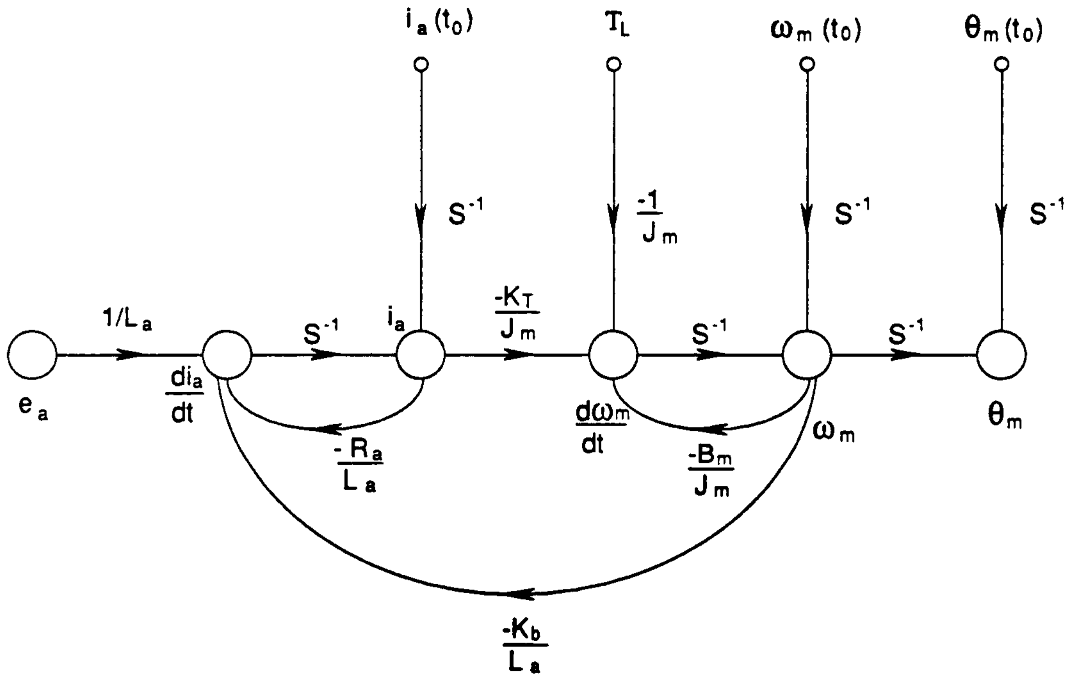

Figure 2.3

State diagram of the modeled motor

b. Transfer Function

Taking the Laplace transform of Equations 2.3 through 2.6, we obtain:

$$T_m = K_T I_a \tag{2.10}$$

$$E_b = K_b \Omega_m \tag{2.11}$$

$$E_a = (R_a + S L_a) I_a + E_b \tag{2.12}$$

$$T_m = (B_m + S J_m) \Omega_m \tag{2.13}$$

where $T_L = 0$ for now.

$$\theta_m = \frac{1}{S} \Omega_m \tag{2.14}$$

To find the transfer function $\frac{\Omega_m}{E_a}$, combine Equation (2.11) with Equation (2.12) and Equation (2.10) with Equation (2.13) .

$$E_a = (R_a + S L_a) I_a + K_b \Omega_m$$

$$K_T I_a = (B_M + S J_m) \Omega_m .$$

Combining the last two equations gives us

$$E_a = (R_a + S\,L_a)\,\frac{(B_m + S\,J_m)\,\Omega_m}{K_T} + K_b\,\Omega_m$$

$$\frac{\Omega_m}{E_a} = \frac{K_T}{(R_a + S\,L_a)(B_m + S\,J_m) + K_b\,K_T}$$

$$\frac{\Omega_m}{E_a} = \frac{K_T}{L_a\,J_m\,S^2 + (R_a\,J_m + B_m\,L_a)S + (K_B\,K_T + R_a\,B_m)} \qquad (2.15)$$

Using $\theta_m = \frac{1}{S}\,\Omega_m$,

$$\frac{\theta_m}{E_a} = \frac{K_T}{L_a\,J_m\,S^3 + (R_a\,J_m + B_m\,L_a)S + (K_B\,K_T + R_a\,B_m)s} \qquad (2.16)$$

The block diagram representation of the DC motor system is drawn in Figures 2.4(a, b, c) . The advantage of using the block diagram is that it gives a clear picture of the transfer function relation between each block of the system.

Although a DC motor by itself is basically an open-loop system, the state diagram and the block diagram show that the motor has a built-in feedback loop caused by the back emf . Physically, the back emf represents the feedback of a signal that is proportional to the negative of the speed of the motor. As seen before, the back emf constant K_b represents an added term to the resistance R_a and viscous-friction coefficient B_m.

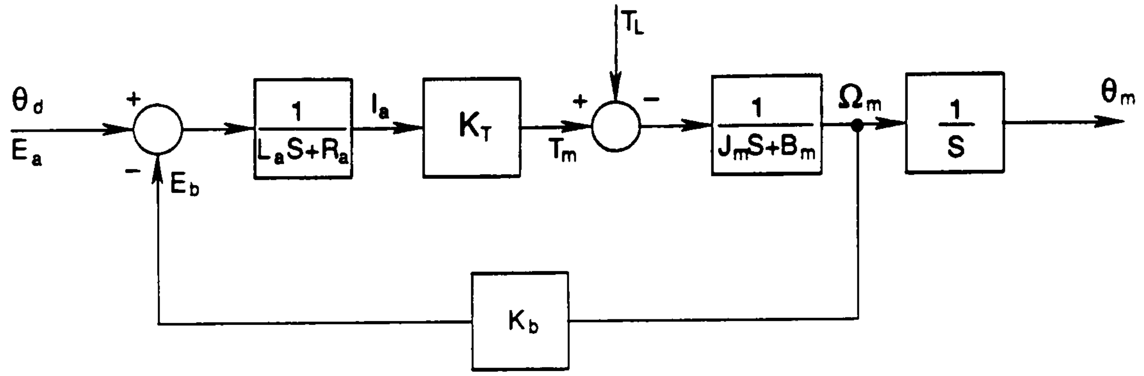

Figure 2.4(a)

Block diagram of the model motor

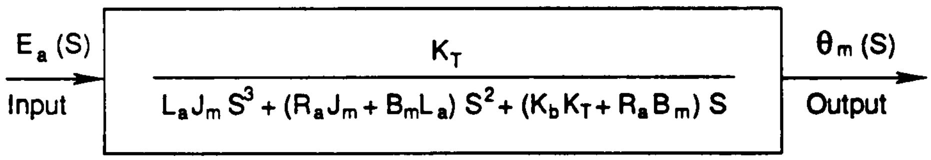

Figure 2.4(b)

Block diagram of motor transfer function

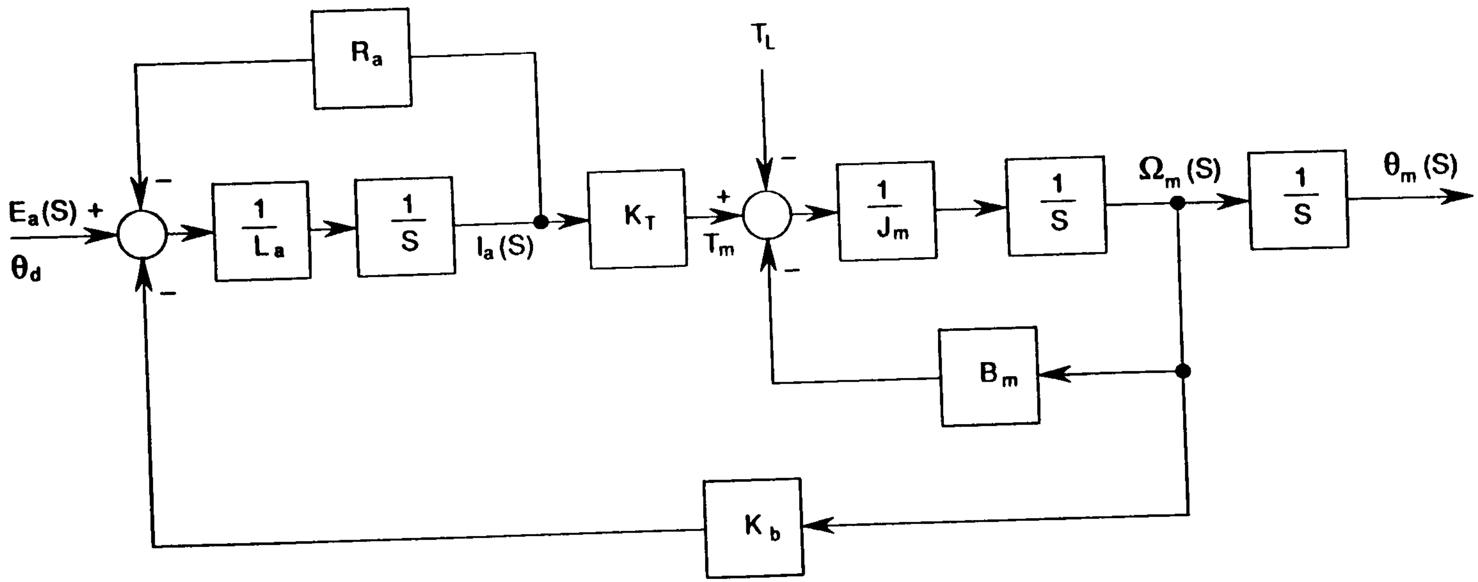

Figure 2.4(c)

Block diagram of the modeled motor

Although functionally the torque constant and the back emf constant are two separate parameters, their values are closely related.

The mechanical power developed in the motor armature is

$$P = T_m(t) \cdot W_m(t) = e_b(t) \cdot i_a(t) = K_b \cdot W_m(t) \cdot T_m(t)/K_T$$

from which

$$K_b(\text{v/rad/sec}) = K_T(\text{N . m/A}) .$$

Thus, the values of K_b and K_T are identical in using the SI unit system, which is the thesis topic case. Then, the transfer function may use:

$$K_b = K_T = K = \text{constant}$$

and the transfer function becomes

$$\theta_m/E_a = \frac{K}{L_a J_m S^3 + (R_a J_m + B_m L_a)S^2 + (K^2 + R_a B_m)S} \tag{2.17}$$

2.5. Modeled Motor Parameters Calculations

After finding the transfer function of the modeled motor, the physical parameters are found experimentally by testing the motor. The instruments used to perform the experiments are:

a) DM-100 Hampden DC machine, which operates either as a motor or as a generator;

b) DYN-100-DM Dynamometer operating like a motor.

Power Required:

0-150 volt variable DC , 1 amp .

0-125 volt variable DC , 5 amps.

Meters Required:

0-150 volt DC voltmeter

0-0.5 amp DC ammeter

0-1.0 amp DC ammeter.

Additional Material Required:

MGB Bed-Plate

SLA-100 Strobe-tachometer.

The modeled motor used to drive the radar antenna is a DM-100 Hampden DC machine.

The value of the armature resistance is found by conducting the following experiment.

Connecting the power supply as shown below in Figure 2.5, the voltage is slowly increased until the ammeter reads 1.0 amp armature current. The corresponding voltage is 4 volts.

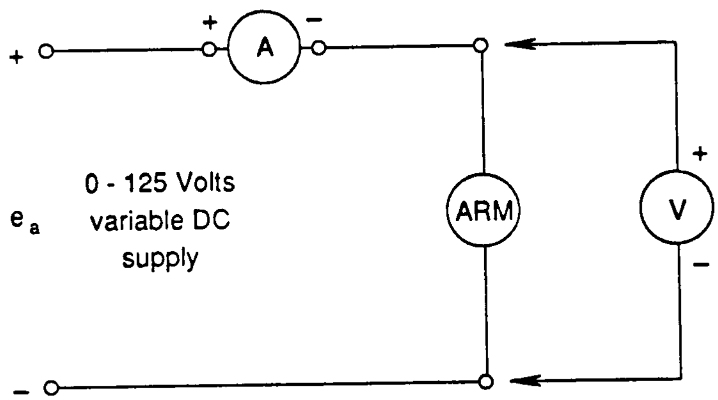

Figure 2.5

Connections setup for the tested motor

$$R_a = \frac{V_a}{I_a} = \frac{4}{1} = 4\Omega$$

The value of the armature inductance is measured by using a Hewlett Packard LCR meter impedance bridge. Four readings were taken at four different shaft positions 90° apart. The average of the four readings is to determine the armature inductance, L_a.

$$L_a = \frac{La_1 + La_2 + La_3 + La_4}{4}$$

$$= \frac{2710^{-3} + 2410^{-3} + 2610^{-3} + 2310^{-3}}{4} = 2510^{-3}\ H$$

The back emf constant or voltage constant, K_b , can be found by running the tested DM-100 Hampden motor as a generator driven by another DYN-100-DM motor. While measuring the generated voltage at the generator armature, the corresponding shaft speed of the generator is also being measured by a strobe tachometer. The back mmf constant is then obtained by the following relationship:

$$K_b = \frac{E_a}{W_m} \left(\frac{V}{RPM}\right)$$

A typical setup of the experiment connection is shown below in Figure 2.6. The two machines are placed on the bedplate and are coupled tightly by a rubber coupling. The motor is operated as a DC shunt motor and the generator is operated as a separately excited generator which is the thesis case. Data is recorded in Table 2.1 for different speeds correspond to different terminal voltages which also correspond to different loads at the generator terminals.

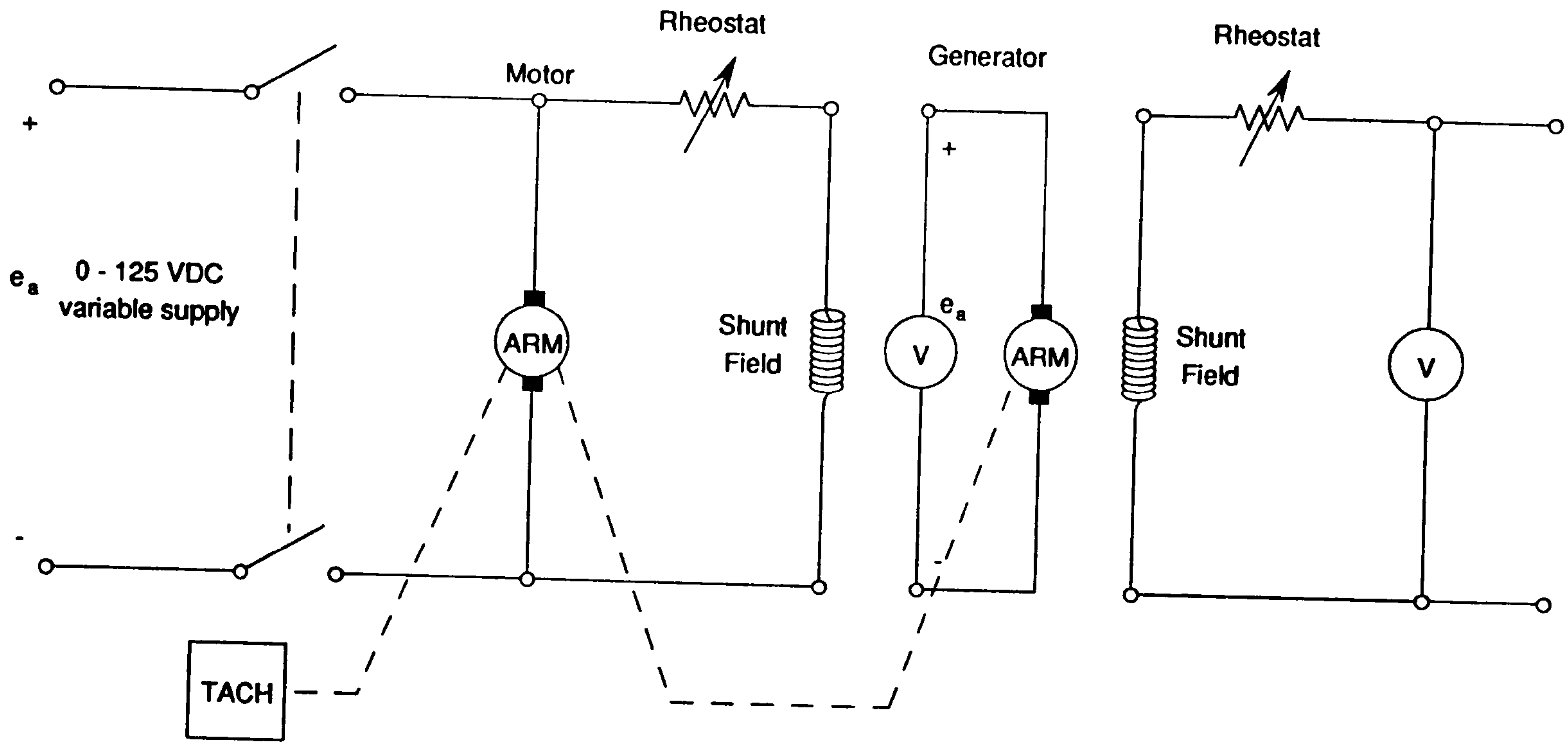

Figure 2.6

Setup connection for the tested motor

Speed (RPM)	600	900	1200	1500
Voltage (volts)	42	68	84	98
K_b $\frac{\text{volts}}{\text{RPM}}$	.070	.075	.007	.065

TABLE 2.1.

VALUES OF VOLTAGES FOR THEIR CORRESPONDING SPEED

$$K_b \text{ Average} = \frac{.07 + .075 + .007 + .065}{4} = .07 \frac{v}{\text{RPM}}$$

$$K_b = .07 \frac{v}{\text{RPM}} \times \frac{60}{2\pi} = .65 \frac{\text{volt sec}}{\text{Rad}}$$

Since the SI units are used, the torque constant, K_T, is equal to the back emf constant

$$K_T = K_b = .65 \quad \text{(Newton . meter/Amp)}$$

The moment of inertia is obtained from the manufacture, Hampden Engineering Corporation. The given value,

$$J_m = .054\ \ell b - ft^2$$

$$= .054\ \ell b ft^2 \frac{.45\ kg}{\ell b} \cdot \frac{.09 m^2}{ft^2} = 2.25 \times 10^{-3}\ kgm^2$$

The viscous frictional coefficient, B_m , is measured by finding the mechanical loss of the machine. This mechanical loss includes the windage and friction loss such as bearing friction, friction of the brushes on the commuator, and air resistance. All these factors produce a mechanical drag on the machine. The same set up used in the experiment to find the back mmf constant is also used to find the mechanical losses. The tested DM-100 Hampden motor is running as a generator driven by the DYN-100-DM motor, as shown in Figure 2.6. The mechanical loss is equal to the difference of the power drawn by the motor to drive the unloaded generator, P_{ug} , and the power drawn by the motor to drive or run itself only, P_m . Since the generator is not loaded, there was no power loss in the armature winding. Also, the power loss in the field of the generator does not come from the motor, separately excited generator. Therefore, the extra power used to drive the generator was all mechanical power loss.

$$P_{\text{mechanical loss}} = V_{ug} \cdot I_{ug} - V_m I_m$$

The measured voltages and their corresponding currents at speed of 1800 RPM are given by:

$$P_{\text{mechanical loss}} = 125 \times 1 - 125 \times \cdot .6 = 50 \text{ watts.}$$

$$T = B_m W_m$$

$$B_m = \frac{T}{W_m} = \frac{P/W_m}{W_m} = \frac{P}{W_m^2}$$

$$Bm = \frac{50}{(1800\ RPM)^2} = \frac{50}{(1800 \times \frac{2\pi}{60})^2} = 1.4 \times 10^{-3}\ \frac{N\ sec}{m} \quad .$$

CHAPTER III

CONTROL DESIGN FOR MODELED SYSTEM

3.1. Introduction

In this chapter the design of control system will be carried out using the classical method and the modern method. These controllers are designed so that they will meet the desired given specifications for the system. The given specifications are the velocity error constant, K_v equal to 20 and the phase margin, PM of 45°. The design of the classical controller is done by using the frequency-domain and the transfer function approaches. The frequency-domain techniques utilize the Bode diagrams that are now applied to the design of linear control system. The modern controller is done by using the linear quadratic optimum control method which uses the time domain and the state variable approach. Modern control deals with the optimization of system performance. This method was discovered and applied to the control systems analysis and design very recently. But, the theory behind this new control method had been always there in the special form of the calculus of variation [4]. Vectors and matrices are used extensively in the linear quadratic method. In design problems, the difficulties lie in the fact that there are no unified methods of arriving at a designed system given the time-domain specifications, such as peak overshoot, delay time, rise time, settling time, and so on. On the other hand, there are many methods available in frequency-domain, such as the Bode plot method which is chosen here because it is more practical and also the specifications are in terms of in the Bode diagram. Two types of compensation controls are used in this project, one with series compensation using phase-lead and phase-lag network compensators and the other one is an inner loop-outer loop feedback compensation using phase-lag compensator. It is important to realize that once the analysis and design are carried out in the frequency-domain, the time-domain properties of the system can be interpreted based on the relationships that exist between the time-domain and the frequency-domain characteristics.

To investigate the effect of feedback on the various aspects of system performance, are investigated. We start with the input-output relation of the control system [5]; see Figure 3.1.

$$M = \frac{C}{R} = \frac{\text{Output}}{\text{Commad Input}} = \frac{G}{1 + GH} \tag{3.1}$$

From Equation 3.1, feedback affects the gain G an open-loop system by a factor of $1 + GH$. In a practical control system, G and H are functions of frequency, so the magnitude of $1 + GH$ may be greater than 1 in one frequency range but less than 1 in another. Therefore, feedback could increase the gain of the system in one frequency range but decrease it in another.

Stability is a concept that describes whether the system will be able to follow the input command. A system is said to be unstable if its output is out of control or increases without bound. At least one root of its characteristic equation $(1 + G(s)\,H(s) = 0)$ lies on the right-half side of the S plane.

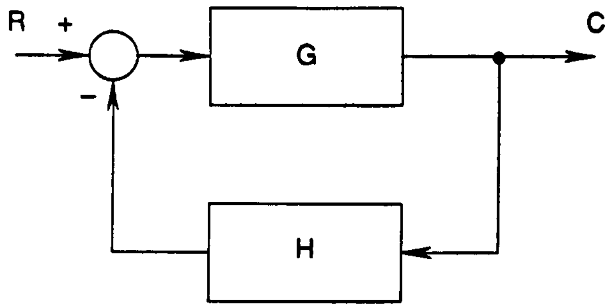

Figure 3.1

Feedback system block diagram

Sensitivity considerations often play an important role in the design of control systems. Since all physical elements have properties that change with environment and age, the parameters of a control system cannot always be considered completely stationary over the entire operating life of the system. A good control system should be very insensitive to parameter variations while still able to follow the command input responsively. The sensitivity of the gain of the overall system M to the variation in G is defined as,

$$S_G^M = \frac{\partial_M/M}{\partial_G/G} \tag{3.2}$$

where ∂_M is the incremental change in M due to the incremental change in G ; $\frac{\partial_M}{M}$ and $\frac{\partial_G}{G}$ are the percentage changes in M and G , respectively.

$$S_G^M = \frac{\partial M}{\partial G}\frac{G}{M} = \frac{1}{(1+GH)^2} \cdot \frac{G}{\frac{G}{1+GH}} = \frac{1}{1+GH} \tag{3.3}$$

This relation in Equation 3.3 shows that the sensitivity function can be made arbitrarily small by increasing GH , provided that the system remains stable.

All physical control systems are subject to some types of noise during operation such as the thermal noise voltage in electronic amplifiers, brush or commutator noise in DC motors, and other places. The effect of feedback on noise depends greatly on where the noise is introduced into the system. However, in many situations, feedback can reduce the effect of noise on system performance by a factor of $1 + GH$.

Also, feedback has effects on such performance characteristics as bandwidth, impedance, transient response, and frequency response. Feedback control systems may be classified in a number of ways, depending upon the purpose of the classification. For instance, according to the method of analysis and design, feedback control systems are classified as linear and nonlinear, time varying or time invariant. According to the types of signal found in the system, reference is often made to continuous-data and discrete-data systems, or modulated and unmodulated systems. Refering to the type of system components, systems are classified such as electromechanical control systems, hydraulic control systems, biological control systems. Control systems are often classified according to the main purpose of the system such as a positional control system and a velocity control system.

For the classification made according to the methods of analysis and design, linear systems do not exist in practice. Since all physical systems are nonlinear to some extent, linear feedback control systems are idealized models that are fabricated purely for the simplicity of analysis and design. When the magnitudes of the signals in a control system are limited to a range in which system components exhibit linear characteristics (the principle of superposition applies), the system is essentially linear. But when the magnitudes of the signals are extended outside the range of the linear operation, depending upon the severity of the nonlinearity, the system should no longer be considered linear. For instance, amplifiers used in control systems often exhibit saturation effects when their input signals become large; the magnetic field of a motor usually has saturation properties, the rotational frictions encountered in physical systems are usually of a nonlinear nature, and many more. Linearizing the control system, there exist many analytical and graphical techniques for design and analysis purposes. However, nonlinear systems are very difficult to treat mathematically, and there are no general methods that may be used to solve a wide class of nonlinear systems. When the parameters of a control system are constant with respect to time during the operation of the system, the system is called a time-invariant system. In practice, most physical systems contain elements that vary with time. For example, the winding resistance of the motor will vary when the motor temperature is rising. Although a time-varying system without nonlinearity is still a linear system, the analysis and design of this class of systems are usually much more complex than that of the linear time-invariant systems.

Since time is used as an independent variable in most control systems, it is usually of interest to evaluate the state and output responses with respect to time, or simply the time response. In the analysis problem, a reference input signal is applied to the system, and the performance of the system is evaluated by studying the system response in the time domain. Therefore, in most control system problems the final evaluation of the performance of the system is based on the time responses. The time response of a control system is usually divided into two parts: the transient response and the steady-state response. It can also be stated that the steady state response is that part of the response which remains after the transient response has died out. All control systems exhibit transient phenomenon to some extent before a steady state is reached. Since inertia, mass, and inductance cannot be avoided entirely in physical systems, the responses of a typical control system cannot follow instantaneously sudden changes in the input, and transients are usually observed.

Therefore, the control of the transient response is necessarily important, as it is a significant part of the dynamic behavior of the system, and the deviation between the output response and the input or the desired response, before the steady state is reached, must be closely watched. The steady-state response is also very important, since when compared with the input, it gives an indication of the final accuracy of the system. If the steady-state response of the output does not agree with the steady-state of the input exactly, the system is said to have a steady-state error. A component of this steady-state error, which is unavoidable, is caused by the nonlinear elements of the system. Unlike many electrical circuits and communication systems, the input excitations for the radar tracking system are not known ahead of time because the position of the target to be tracked may vary in an unpredictable manner, so that they cannot be expressed mathematically. This makes it difficult to design the control system so that it will perform satisfactorily to any input signal. For the purposes of analysis and design, it is necessary to assume some basic types of input functions so that the performance of the tracking system can be evaluated with respect to these test signals. By selecting these basic test signals properly, the responses due to these inputs allow the prediction of the system's performance to other more complex inputs. Some of these test signals are step input, ramp input, and parabolic input function. The test signal used to test the performance of the designed control system is the unit-step input or ramp input function. So, for every design method, there is a unit-step response or ramp response for the system.

3.2. Classical Method Design Using Bode Plot

After finding the values of physical parameters of the modeled motor in section 2.5, these values are substituted in the transfer function of the system, $\frac{\theta_m}{E_a}$. Those values are listed below.

$R_a = 4$ ohms

$L_a = 25 \times 10^{-3}$ Henry

$K_b = K_T = 0.65$ (volt.sec/rad; Newton . meter/Amp)

$J_m = 2.25 \times 10^{-3}$ Kg m^2 ,

J_m total = $6 \times 2.25 \times 10^{-3}$ K_g m^2 , including the antenna load inertia

$B_m = 1.4 \times 10^{-3}$ Newton · sec/m

B_m total = $6 \times 1.4 \times 10^{-3}$ N. sec/m, including the antenna load viscous coefficient

Using Equation 2.16,

$$\frac{\theta_m}{E_a} = \frac{K_T}{L_a J_m s^3 + (R_a J_m + B_m L_a)s^2 + (K_b K_T + R_a B_m)s}$$

$$\frac{\theta_m}{E_a} = \frac{.65}{3.375\ 10^{-4}\ s^3 + .0542\ s^2 + .456\ s}$$

$$\frac{\theta_m}{E_a} = \frac{1926}{s(s^2 + 160s + 1350)}$$

$$\frac{\theta_m}{E_a} = \frac{1926}{s(s+9)(s+151)} \qquad (3.4a)$$

$$\frac{\theta_m}{E_a} = \frac{1.42}{s(1 + \frac{s}{9})(1 + \frac{s}{151})} \tag{3.4b}$$

$$G\ plant = G_p = \frac{\theta_m}{E_a} = \frac{1.42}{s(1 + .11\ s)(1 + .0066\ s)} \tag{3.4c}$$

The steady state error of the system depends on the input and the type of the system. In control systems, the error signal is equal to the difference of the reference input $e_a(t)$ and the controlled output $\theta_m(t)$. To compare between these two signals, they must be dimensionally the same. This is so in this case because the controlled output $\theta_m(t)$ is negatively fed back to the input through a potentiometer that converts the angular displacement of the motor shaft into its correspondent voltage. The transfer function of this potentiometer is unity. Therefore, the system is a unity feedback control system and shown in Figure 3.2.

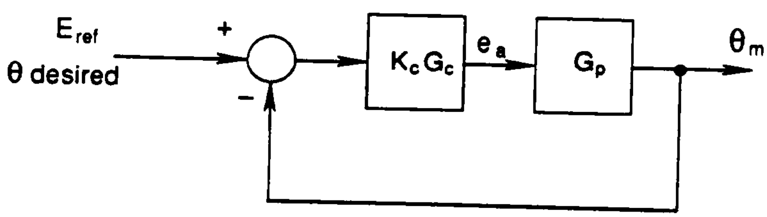

Figure 3.2

Control system block diagram

The smaller the error is, the closer the controlled output follows the desired input, where G_p is the transfer function of the modeled motor. $K_c\, G_c$ is the transfer function of the series compensation controller which is going to be designed using phase-lead and then phase-lag networks so that the given specifications are met. After that, an inner loop-outer loop feedback compensation controller is designed using a phase-lag network.

$$e(t) = e_a(t) - \theta_m(t)$$

By using the final-value theorem, the steady state error is

$$ess = \lim_{t\to\infty} e(t) = \lim_{s\to\infty} SE(s)$$

where $E(s) = E_a(s) - \theta_m(s) = \dfrac{E_a(s)}{1+G_p(s)}$, ignoring K_cG_c for now.

$$ess = \lim_{s\to 0} \frac{s\, E_a(s)}{1+G_p(s)} \tag{3.5}$$

For $E_a(s)$ as a step input, and a type one system,

$$ess = \lim_{s\to 0} \frac{s\frac{A}{s}}{1+G_p(s)} = \frac{A}{1+\lim\limits_{s\to 0} G_p(s)} = \frac{A}{1+\lim\limits_{s\to 0} \dfrac{1.42}{s(s+9)(s+151)}} = 0,$$

which is very desirable.

For $E_a(s)$ is as ramp input, and a type one system,

$$E_a(s) = \frac{A}{s^2}$$

$$ess = \lim_{s \to 0} \frac{s \frac{A}{s^2}}{1 + \lim_{s \to 0} s\, G_p(s)} = \frac{A}{\lim_{s \to 0} G_p(s)} = \frac{A}{K_v}$$

where $K_v = \lim_{s \to 0} s\, G_p(s)$, velocity error constant which is specified to be equal to 20 .

For $e_a(t)$ a unity ramp input, $A = 1$,

$$ess = \frac{1}{K_v} = \frac{1}{20} = .05$$, considerably small error.

For the given G_p ,

$$K_v = \lim_{s \to 0} s\, G_p(s) = \frac{1926}{9 \times 151} = 1.42$$

For the control system to have $K_v = 20$, the gain is raised by factor of $\frac{20}{1.42} = 14.1 = K_c$, which is the added gain from the series compensator so that the specification $K_v = 20$ is met. Therefore, the adjusted transfer function of the control system is:

$$\frac{\theta_m}{E_a}\text{ adjusted} = \frac{20}{s(1+\frac{s}{9})(1+\frac{s}{151})} \tag{3.6}$$

So, to meet the K_v specification, the adjusted gain (K_c) is set to be 14.1 . Thereafter, a series compensator is inserted in the system in order to meet the phase margin specification of 45° . This series compensator is of the form:

$$G_c = K_c \cdot \frac{1 + aTs}{1 + Ts} = Kc \cdot a \cdot \frac{s + \frac{1}{aT}}{s + \frac{1}{T}} \ .$$

For $a > 1$, a phase-lead compensator is necessary.

For $a < 1$, a phase-lag compensator is used.

To design these compensators, the Bode plot technique is used. The definition of the Bode plot is a plot of the magnitude of the feedback control system gain in dB and the phase of the system gain in degrees versus the sinusoidal input signal frequency or angular velocity, W(rad/sec), on a logarithmic scale. The dB is a measure of the system gain $|G|$, where

$$|G|_{dB} = 20 \log_{10} |G|$$

From the Bode plot, the phase margin (PM) , gain-crossover frequency, and the gain margin are determined. The crossover frequency, f_c or w_c , is the frequency at which the magnitude of the system gain is unity or zero dB. The phase margin is 180° minus the phase angle of the system at the crossover frequency. The gain margin is the magnitude of the system gain at the frequency for which the phase angle of the system gain is $-180°$, where $1 + G(j_W)\,H(j_W) = 0$ or $G(j_W)H(j_W) = -1$. The gain margin is one of the many ways of representing the relative stability of the feedback control system. In principle, a system with a large gain margin should be relatively more stable than one that has a smaller gain margin. Unfortunately, gain margin alone does not sufficiently indicate the relative stability of all systems, especially if parameters other than plant loop gain are variable. In order to strengthen the representation of relative stability of the feedback control system, the phase margin is introduced as a supplement to gain margin. The physical significance of gain margin is the amount of gain in decibels that can be allowed to increase in the system before the closed-loop system reaches instability, and the phase margin becomes zero. Then, the system is marginally unstable. Also, the phase margin is the angle the phase curve must be shifted so that it will pass through the $-180°$ axis at the gain-crossover frequency, so the system becomes marginally unstable. The Bode plot of $G_p(j_W)$, Equation 3.4, is shown in Figure 3.3, using the asymptotic approximation. The phase margin is measured to be 80° and the unit-step response of the feedback system is shown in Figure 3.4. Because the phase margin is relatively high, the feedback system is overdamped with zero overshoot.

The Bode plot of the adjusted system G_p adj, Equation 3.6, is shown on Figure 3.5, where the phase margin has been decreased to 35°. The system is

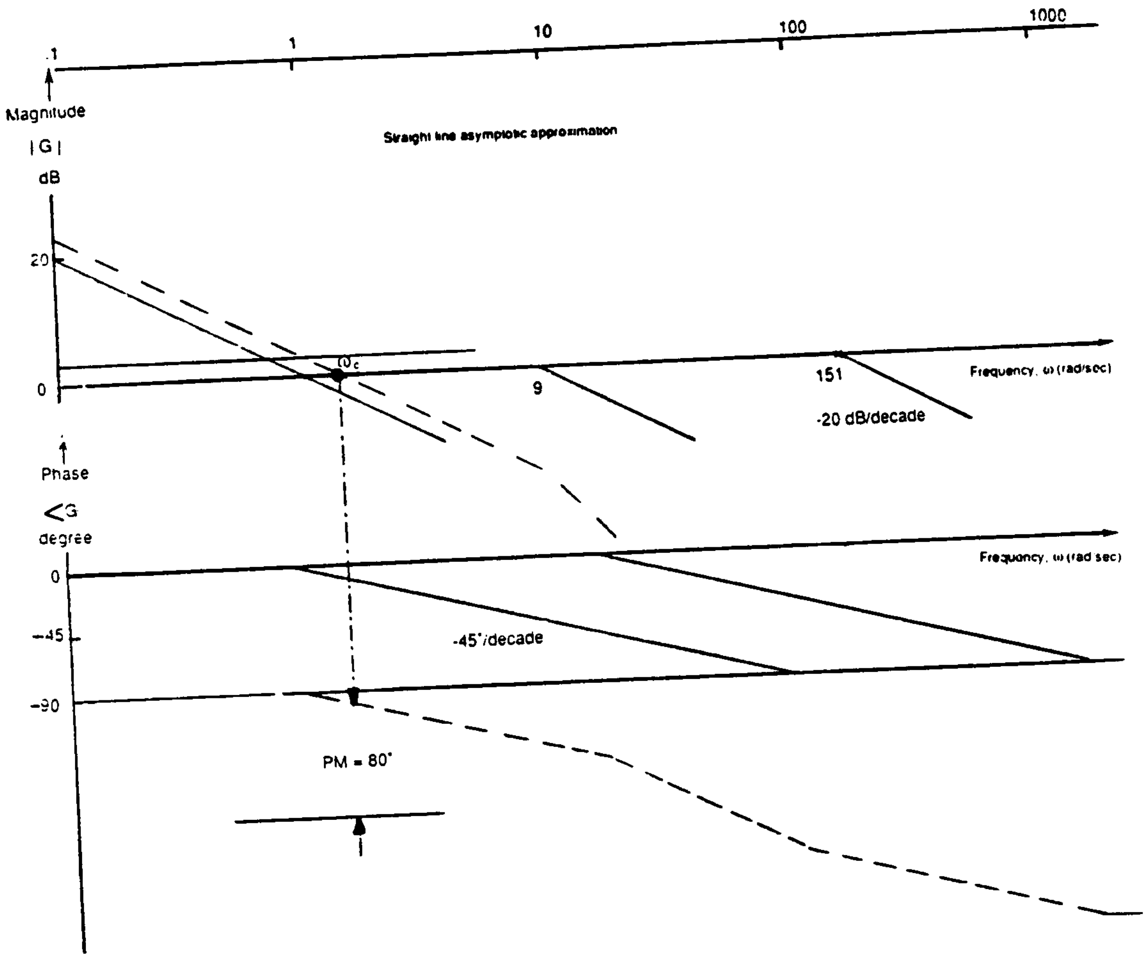

Figure 3.3

Bode plot of uncompensated system

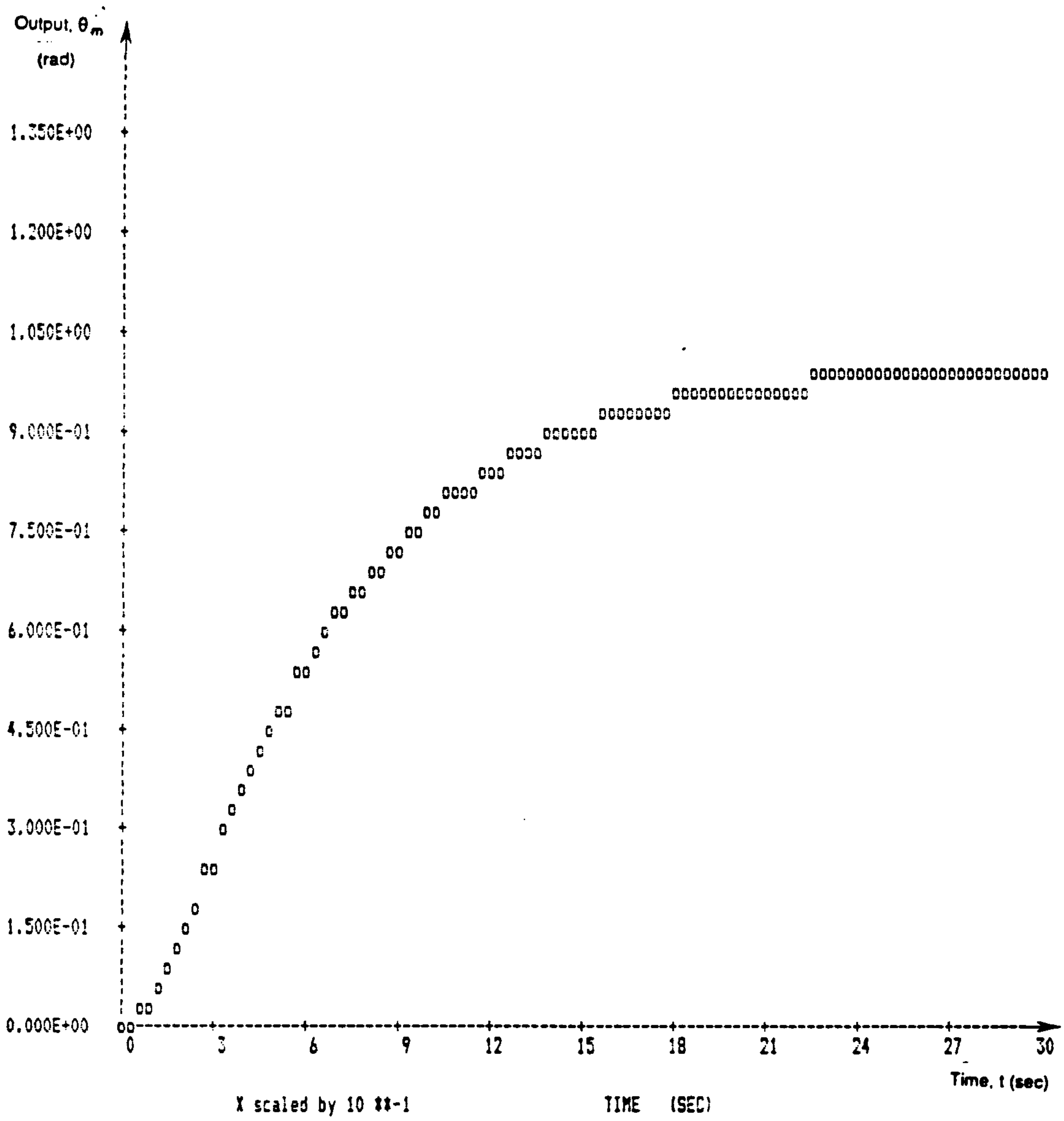

Figure 3.4

Unit-step response of closed-loop uncompensated system output, servomechanism mode

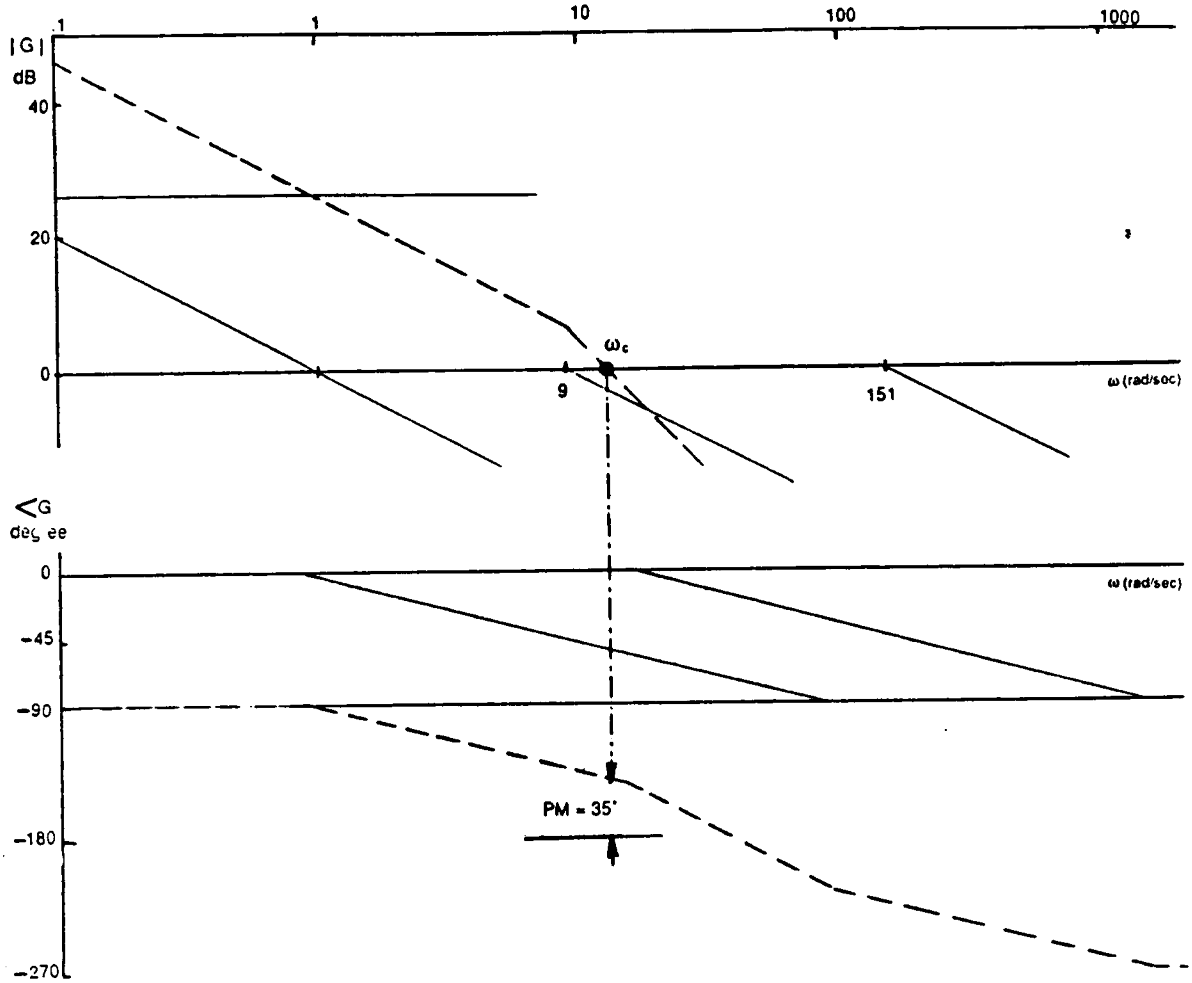

Figure 3.5

Bode plot of adjusted-uncompensated system

still stable but is heading toward instability because the DC gain has been increased in order to decrease the steady state error of the control system. The unit-step response of this adjusted control system is shown on Figure 3.6, where the overshoot is 38% which is relatively high.

The phase margin specification has not been met, so series phase-lead and phase-lag compensators are used to lift the PM from 35° to 45° and more relative stability and less overshoot will occur. Starting with the phase-lead compensation design, which is carried out using the frequency-domain techniques, with the aid of Bode plot. The reason is simply because the affect of compensation is easily obtained by adding its magnitude and phase curves to that of the original system. Using the phase-lead compensation, the function of the network is to increase the phase correspondent to the gain-crossover frequency, while keeping the magnitude curve of the Bode plot relatively unchanged near that frequency. However, usually in phase-lead design, the gain crossover frequency is increased because of the phase-lead network, and the design is essentially finding a compromise between the increase in bandwidth and the desired amount of relative stability or phase margin.

The transfer function of the phase-lead compensator is

$$\frac{E_2(s)}{E_1(s)} = \frac{1 + aTs}{1 + Ts} \quad a > 1$$

where its Bode plot diagram of $\dfrac{E_2(jw)}{E_1(jw)}$ is shown on Figure 3.7 .

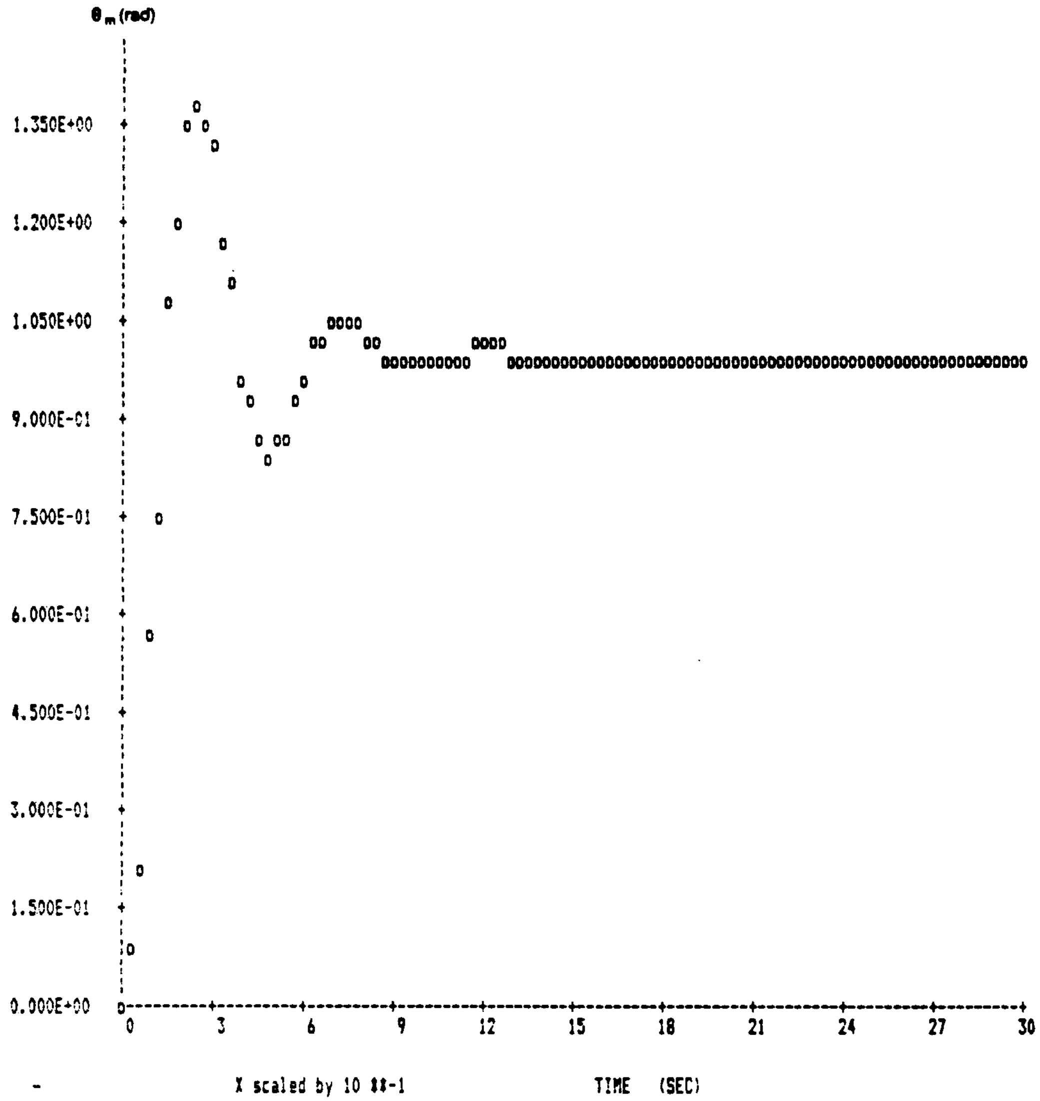

Figure 3.6

Unit-step response of closed-loop adjusted-uncompensated system output, servomechanism mode

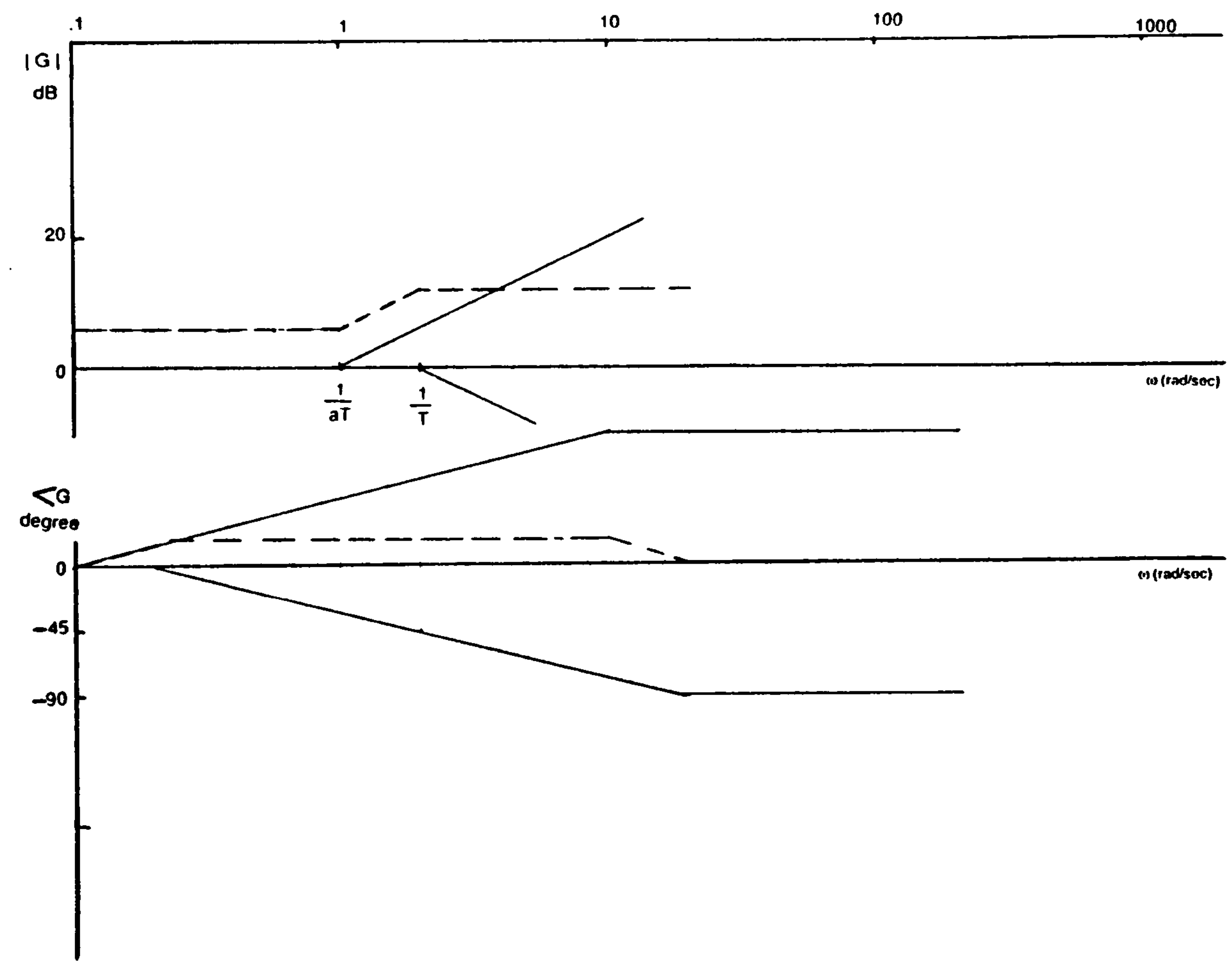

Figure 3.7

Bode plot of phase-lead network

Analytically, ϕ_m and w_m are related to the parameters a and T since w_m is the geometric mean of the two corner frequencies. Therefore,

$$w_m = \frac{1}{\sqrt{a}\,T} \tag{3.7}$$

To determine the maximum phase-lead, ϕ_m , the phase of $E_2(jw)/E_1(jw)$ is written as

$$\phi = \tan^{-1} aTw - \tan^{-1} Tw \Rightarrow \tan\phi = \frac{a\,Tw - Tw}{1 + (a\,Tw)\,(Tw)}$$

when $\phi = \phi_m$,

$$w = w_m = \frac{1}{\sqrt{a}\,T}.$$

Then

$$\tan\phi_m = \frac{(a-1)\left(\frac{1}{\sqrt{a}}\right)}{1+1} = \frac{a-1}{2\sqrt{a}}$$

or

$$\sin\phi_m = \frac{a-1}{a+1} \tag{3.8}$$

The additional amount of phase lead needed to be added to the adjusted system is $45° - 32° = 13°$.

However, by inserting the phase-lead controller, the magnitude curve of the Bode plot is also affected in such a way that the gain-cross-over frequency is shifted to a higher frequency. Although it is a simple matter to adjust the corner frequencies, $\frac{1}{aT}$ and $\frac{1}{T}$, so that the maximum phase of the network, ϕ_m falls exactly at the new gain-crossover frequency, the original phase margin at this point (new w_c) is no longer the same, and could be considerably less. This represents one of the main difficulties in the phase-lead design. In fact, if the phase of the uncompensated system decreases rapidly with increasing frequency near the gain-crossover frequency, phase-lead compensation may become ineffective. So, when estimating the necessary additional amount of phase-lead, it is essential to include some safety margin to account for the inevitable phase dropoff. Therefore,

$$\phi_m = 13° + 6° = 19°,$$

where $6°$ is the added safety margin. Using Equation 3.8,

$$\sin \phi_m = \frac{a - 1}{a + 1}$$

or

$$a = \frac{1 + \sin \phi_m}{1 - \sin \phi_m} = 2$$

To determine the proper location of the two corner frequencies, $\frac{1}{aT}$ and $\frac{1}{T}$, it is known from Equation 3.7 that the maximum phase-lead ϕ_m occurs at the geometrical mean of the corners. To achieve the maximum phase margin with the value already determined, ϕ_m, should occur at the new gain-crossover frequency w'_c, which is not known yet. Thus, the problem now is to locate the two corner frequencies so that ϕ_m occurs at w'_c. This may be accomplished graphically as follows:

a) The zero-frequency attenuation of the phase-lead network is calculated from Figure 3.5:

$$20 \log_{10}^{a} = 20 \log_{10}^{2} = 6 \text{ dB} .$$

b) The geometric mean w_m of the two corner frequencies should be located at the frequency at which the magnitude of the uncompensated system in dB is equal to the negative value in decibels of half of this attenuation. This way, the magnitude plot of the compensated system will pass through the 0 - dB axis at $w = w_m = w'_c$. Thus, w_m should be located at the frequency where,

$$|Gp| = \frac{-6}{2} = -3 \text{ dB}$$

From Figure 3.5, the corresponding frequency found at $G = -3$ dB is $14 \frac{rad}{sec}$. Using Equation 3.7, $w_m = \frac{1}{\sqrt{a}\,T}$ or

$$\frac{1}{T} = \sqrt{a}\, w_m = \sqrt{2} \cdot 14 = 20$$

and

$$\frac{1}{aT} = \frac{1}{2} \cdot 14 = 10$$

so

$$G_c = a\,\frac{s + \frac{1}{aT}}{s + \frac{1}{T}} = 2\,\frac{s + 10}{s + 20} = \frac{1 + \frac{s}{10}}{1 + \frac{s}{20}}$$

The adjusted, compensated open loop transfer function of the control system is,

$$\frac{\theta_m}{E_a} = \frac{20\left(1 + \frac{s}{10}\right)}{s\left(1 + \frac{s}{9}\right)\left(1 + \frac{s}{151}\right)\left(1 + \frac{s}{20}\right)} \qquad (3.9)$$

The Bode plot drawn for Equation 3.9 is shown in Figure 3.8, where PM = 45° and $K_v = 20$. The unit-step response of the control system is shown on Figure 3.9, where the overshoot is equal to 24% , which is accepted.

The phase-lag compensator is designed, which is also carried out using the Bode plot.

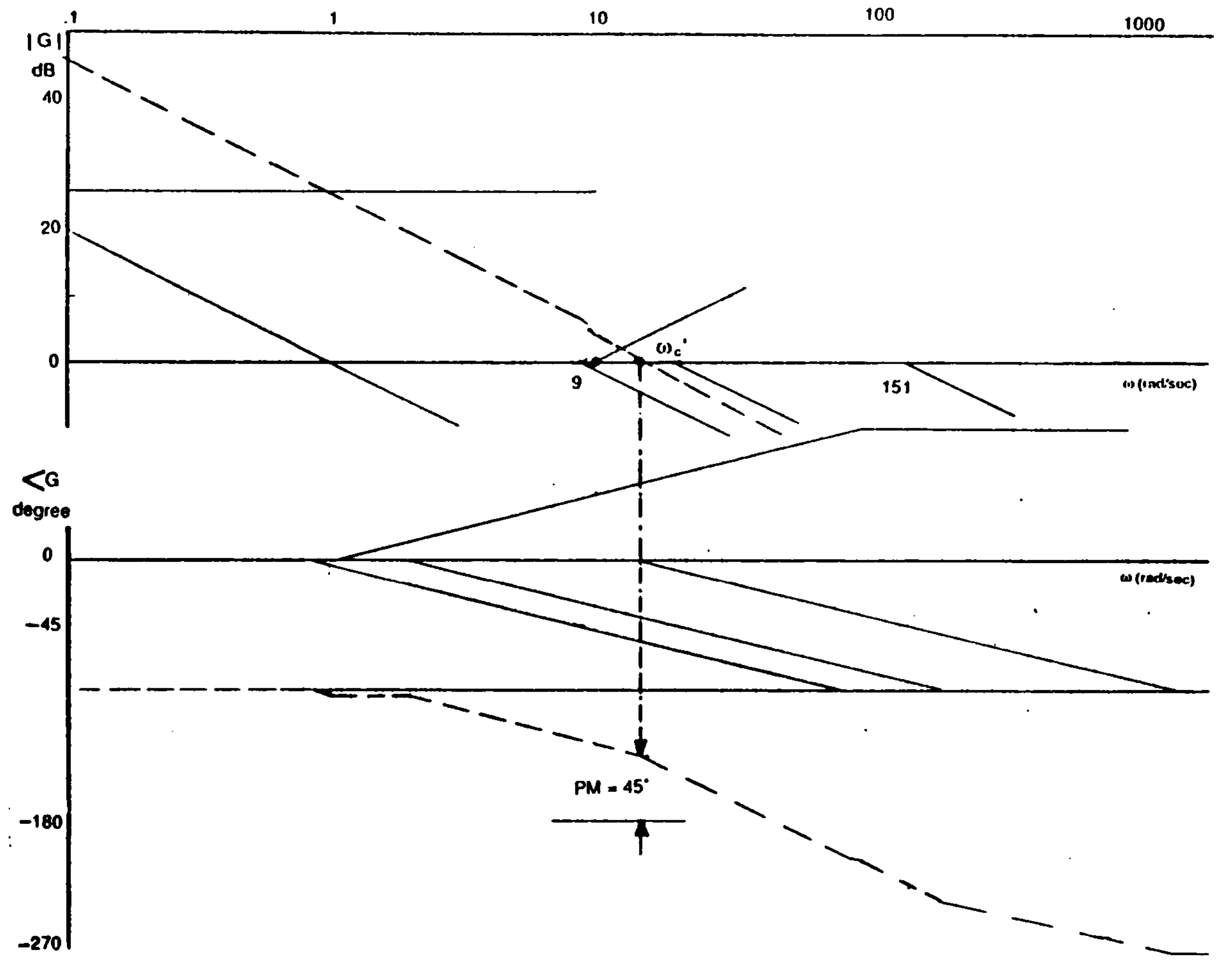

Figure 3.8

Bode plot of compensated system using phase-lead

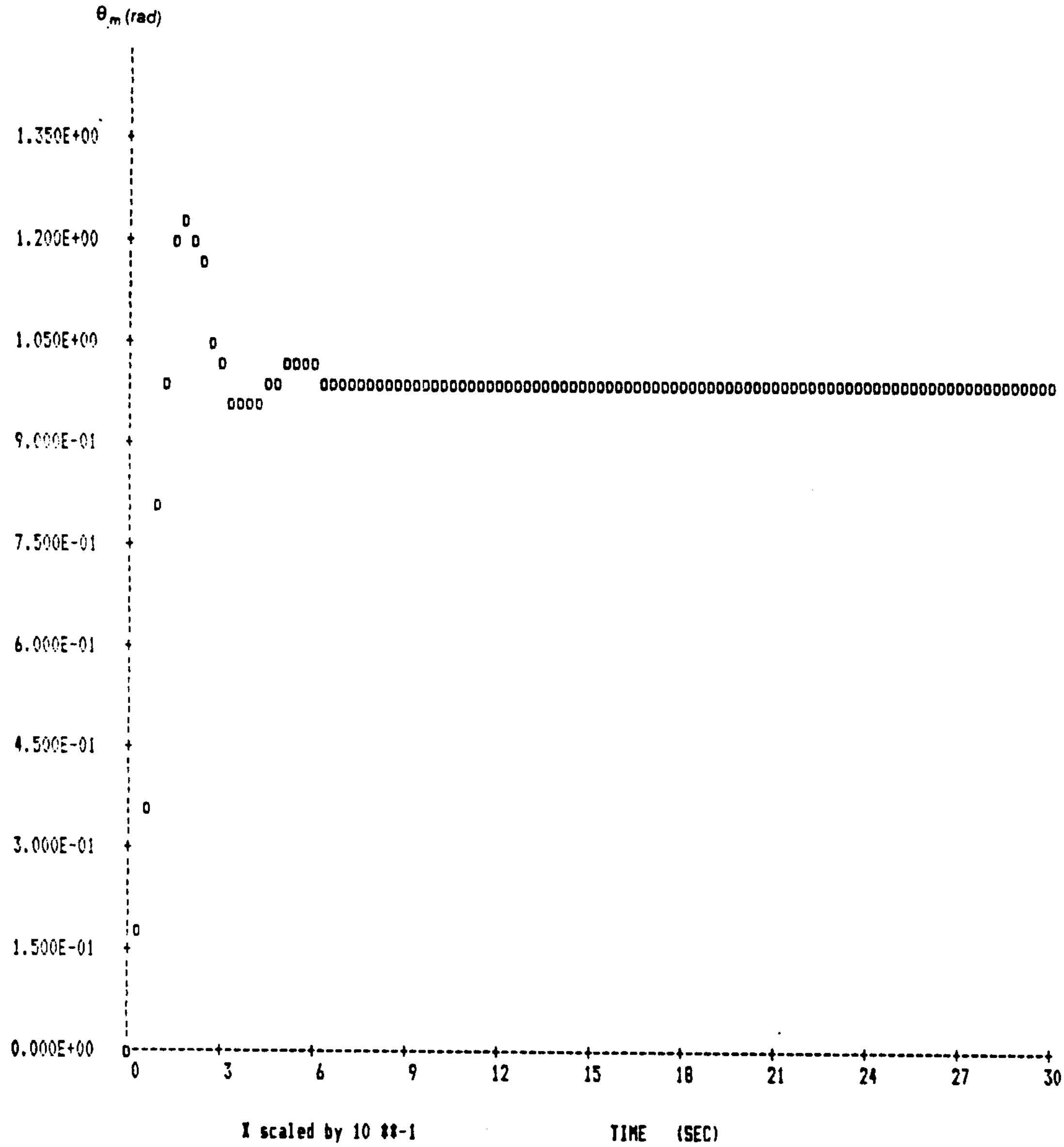

Figure 3.9

Unit-step response of closed-loop compensated system output using phase-lead, servomechanism mode

The transfer function of the phase-lag compensator is

$$\frac{E_2(s)}{E_1(s)} = \frac{1 + aTS}{1 + TS} \qquad a < 1$$

The Bode plot diagram of $\frac{E_2(jw)}{E_1(jw)}$ is shown in Figure 3.10.

The transfer functions of the phase-lead and phase-lag networks are identical in form except for the zero-frequency attenuation and the value of a . Again, the relationship between a and ϕ_m is ,

$$w_m = \frac{1}{\sqrt{a}\,T} \tag{3.10}$$

and

$$\sin \phi_m = \frac{a - 1}{a + 1} \text{ or } a = \frac{1 + \sin \phi_m}{1 - \sin \phi_m} \tag{3.11}$$

Unlike the design of phase-lead compensation, which utilizes the maximum phase lead of the network, the design of the phase-lag compensator utilizes the attenuation of the network at the high frequencies.

In phase-lag compensation, however, the objective is to move the gain-crossover frequency to a lower frequency while keeping the phase curve of the Bode plot relatively unchanged at the gain-crossover frequency.

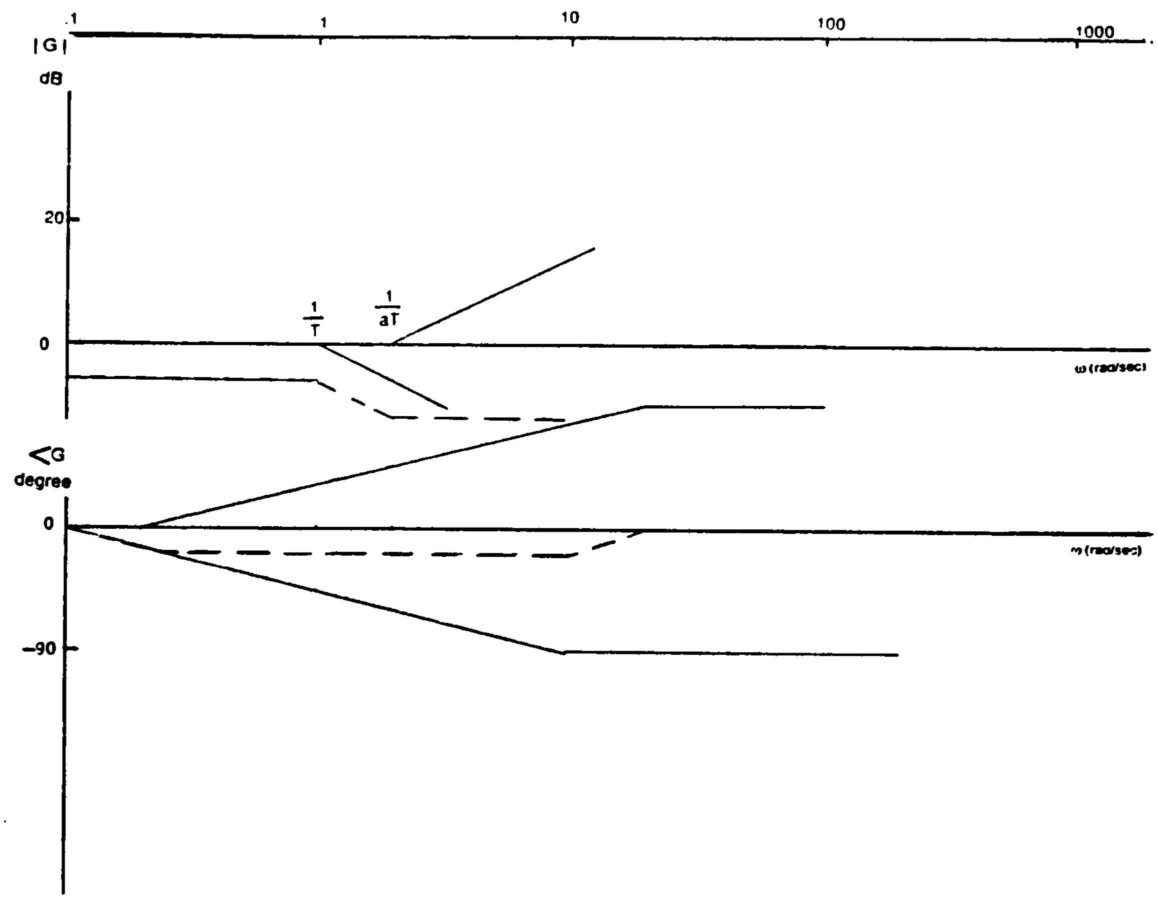

Figure 3.10

Bode plot of phase-lag network

The design procedure for phase-lag compensation, using the Bode plot is outlined as follows. First, it is observed from Figure 3.5 that the desired 45° phase margin can be obtained if the new gain-crossover frequency, w'_c , is at 10 rad/sec. From the magnitude plot, the value of gain system at $w'_c = 10$ rad/sec is 8 dB . This means that the phase-lag controller must provide an attenuation of 8 dB at this frequency. In order to bring the magnitude curve down to the 0 dB-axis at w'_c 10 rad/sec, the value of a is given by

$$20 \log_{10} a = -8 \text{ dB}$$

Therefore,

$$a = .4$$

The value of "a" indicates the required distance between the two corner frequencies of the phase-lag controller, in order that the attenuation of 8 dB is realized. In order that the phase-lag does not appreciably affect the phase curve at the new gain-crossover frequency, the corner frequency $\frac{1}{aT}$ is choosen to be a one decade below w'_c

$$\frac{1}{aT} = \frac{w'_c}{10} = \frac{10}{10} = 1 \text{ rad/sec.}$$

This gives,

$$\frac{1}{T} = a = 0.4$$

so,

$$G_C = a\,\frac{s+\frac{1}{aT}}{s+\frac{1}{T}} = 0.4\,\frac{s+1}{s+0.4} = \frac{1+\frac{s}{1}}{1+\frac{s}{0.4}}$$

The adjusted, compensated open loop transfer function of the control system is:

$$\frac{\theta_m}{E_a} = \frac{20(1+\frac{s}{1})}{s(1+\frac{s}{9})(1+\frac{s}{151})(1+\frac{s}{0.4})} \tag{3.12}$$

The Bode plot drawn for Equation 3.12 is shown in Figure 3.11, where PM = 45° and $K_V = 20$. The unit-step response of the control system is shown on Figure 3.12, where the overshoot is equal to 26% , which is acceptable.

Using the inner loop-outer loop feedback compensation, the angular velocity, W_m is fed back through a tachometer sensor of transfer function equal to 0.1 and the angular displacement is again feed back through a potentiometer sensor with a transfer function equal to one. The block diagram of the inner loop-outer loop feedback compensation system is drawn on Figure 3.13.

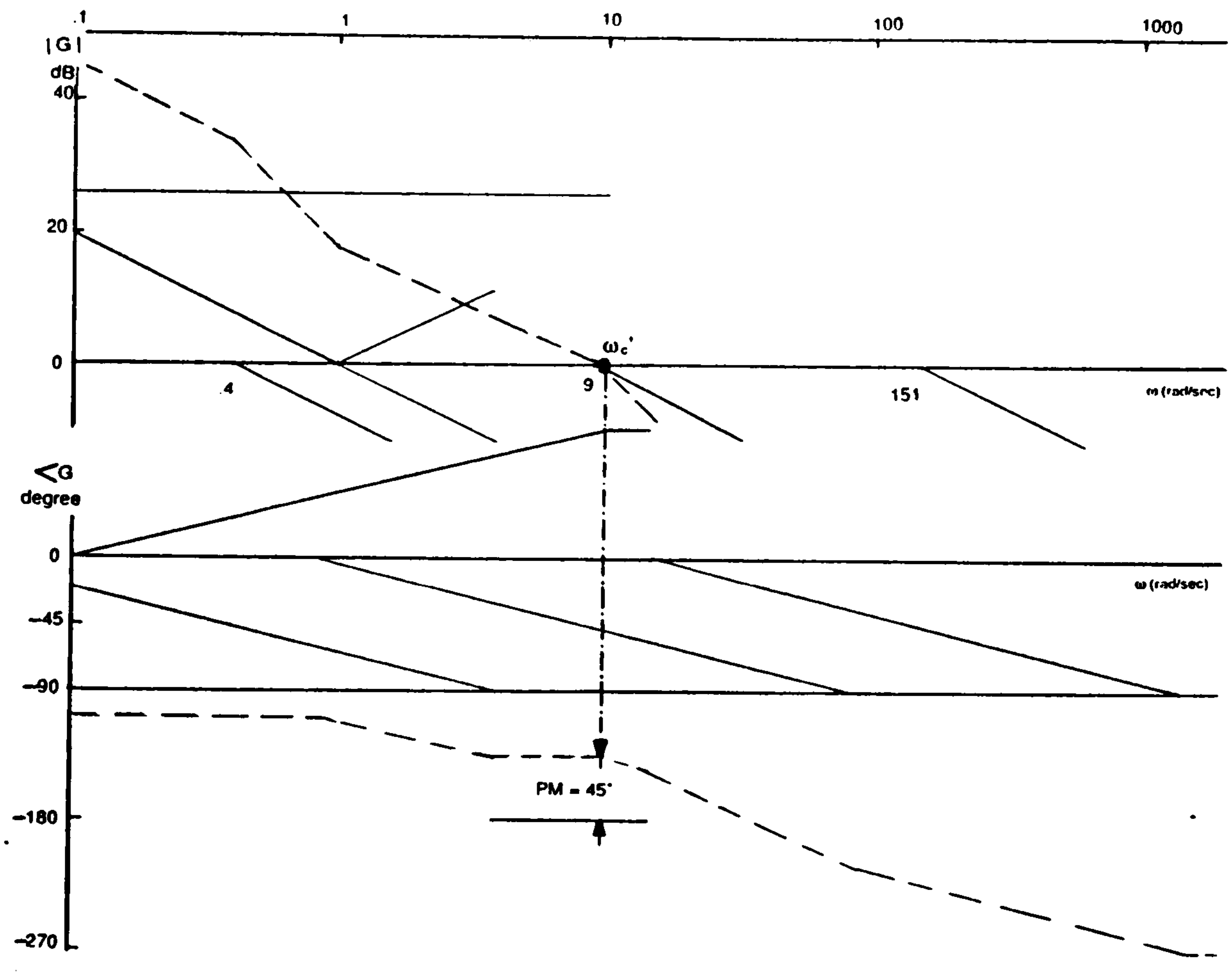

Figure 3.11

Bode plot of compensated system using phase-lag

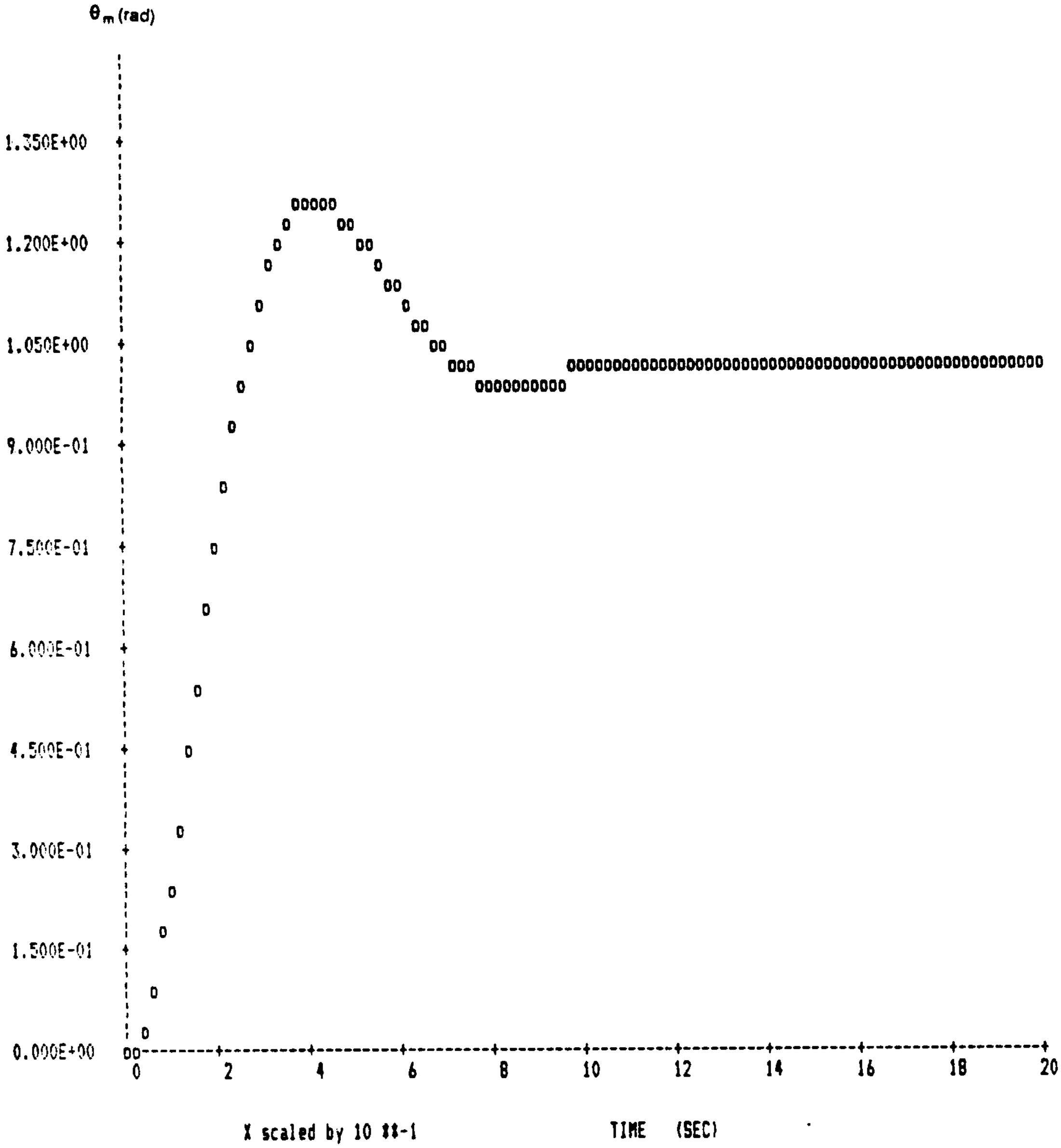

Figure 3.12

Unit-step response of closed-loop compensated system output using phase-lag, servomechanism mode

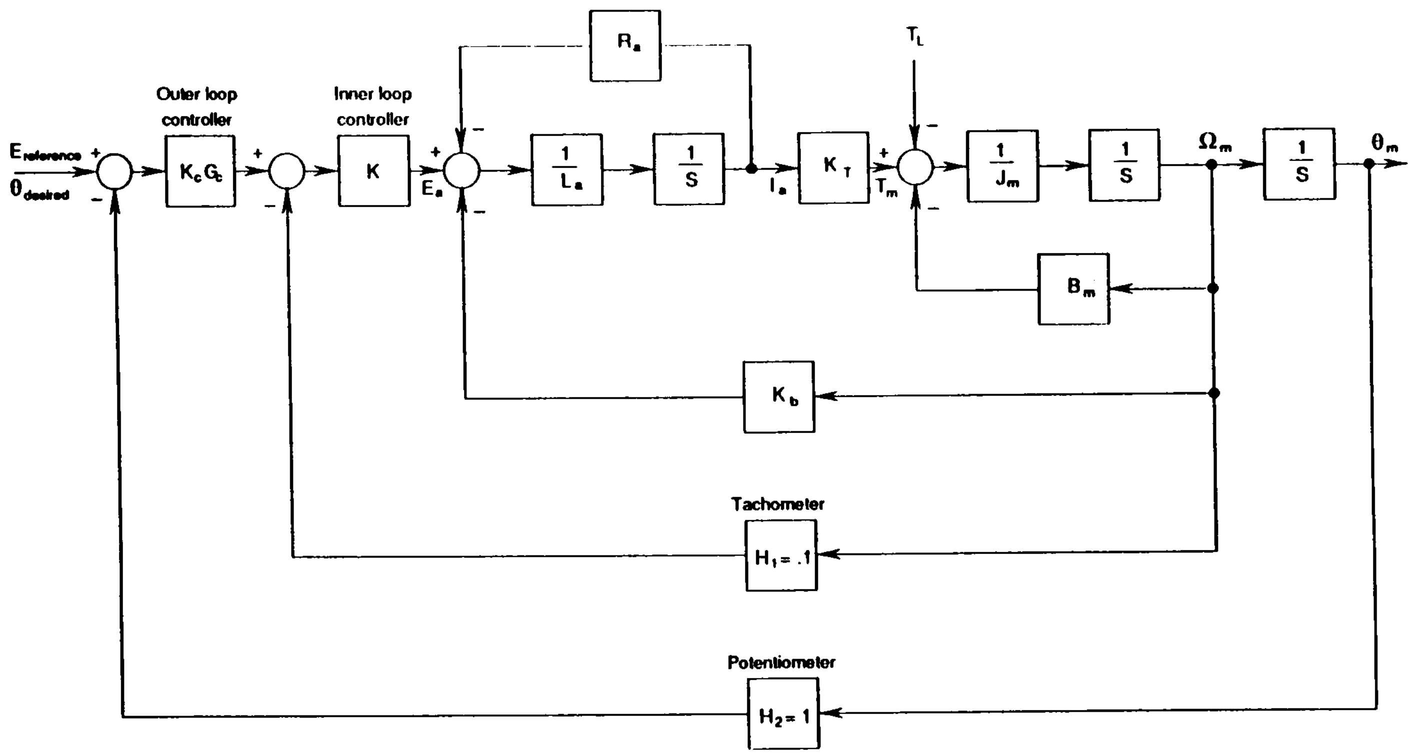

Figure 3.13

Block diagram for the inner loop-outer loop feedback control system

The inner loop is introduced here by inserting the tachometer and the power amplifier into the system to help increase the damping ratio of the system response so that the peak overshoot is decreased. This is done by moving the middle pole of the plant systems characteristic equation further to the left so more system stability will occur.

The inner loop transfer function is:

$$\frac{W_m}{E_i} = \frac{K\,Gp_i}{1 + K\,Gp_i\,H_2}$$

Inserting values gives:

$$\frac{W_m}{E_i} = \frac{\dfrac{K\,1926}{(s + 151)(s + 9)}}{1 + \dfrac{K \times 1926 \times (0.1)}{(s + 151)(s + 9)}}$$

$$\frac{W_m}{E_i} = \frac{1926K}{(s^2 + 160s + 1350) + 192.6K}$$

Then, the inner loop transfer function including the integrator $\frac{1}{s}$, is

$$\frac{\theta_m}{E_i} = \frac{1926K}{s[(s^2 + 160\,s + 1350) + 192.6K]}$$

The outer-open loop transfer function, G , below in Figure 3.14 .

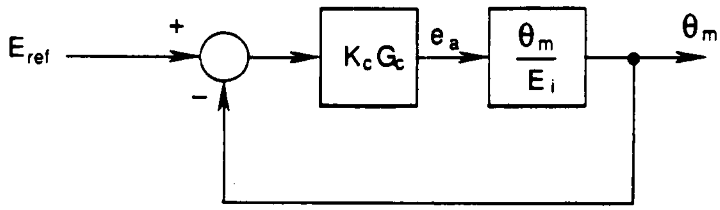

Figure 3.14

Block diagram of the outer loop transfer function

The system characteristic equation is

$$s^2 + 160\,s + 1350 + 192.6K = 0\ .$$

The poles are located at:

$$S = \frac{-160 \pm \sqrt{(20200 - 770.4\,K)}}{2}$$

For different values of K , the correspondent poles are:

For $K = 1 \Rightarrow S = -150\ ; -10$

For $K = 3 \Rightarrow S = -147\ ; -13$

For $K = 5 \Rightarrow S = -144\ ; -16$

Taking $K = 3$, where poles are at $s = -147$ and $s = -13$, the outer-open loop transfer function is:

$$\frac{\theta_m}{E_a} = \frac{5778}{s(s + 147)(s + 13)} \tag{3.13}$$

The velocity constant,

$$K_V = \frac{5778}{147 \times 13} = 3.1$$

$$PM = 80°$$

The unit-step response of Equation 3.13 is shown on Figure 3.15. For $K_V = 21$, $K_C = \frac{21}{3.1} = 6.78$.

$$\frac{\theta_m}{E_a} \text{ adjusted} = \frac{(6.78)(5778)}{s(s + 147)(s + 13)} = \frac{21}{s(1 + \frac{s}{147})(1 + \frac{s}{13})} \tag{3.14}$$

The Bode plot drawn for Equation (3.14) is shown in Figure 3.16, and the unit-step response is shown on Figure 3.17.

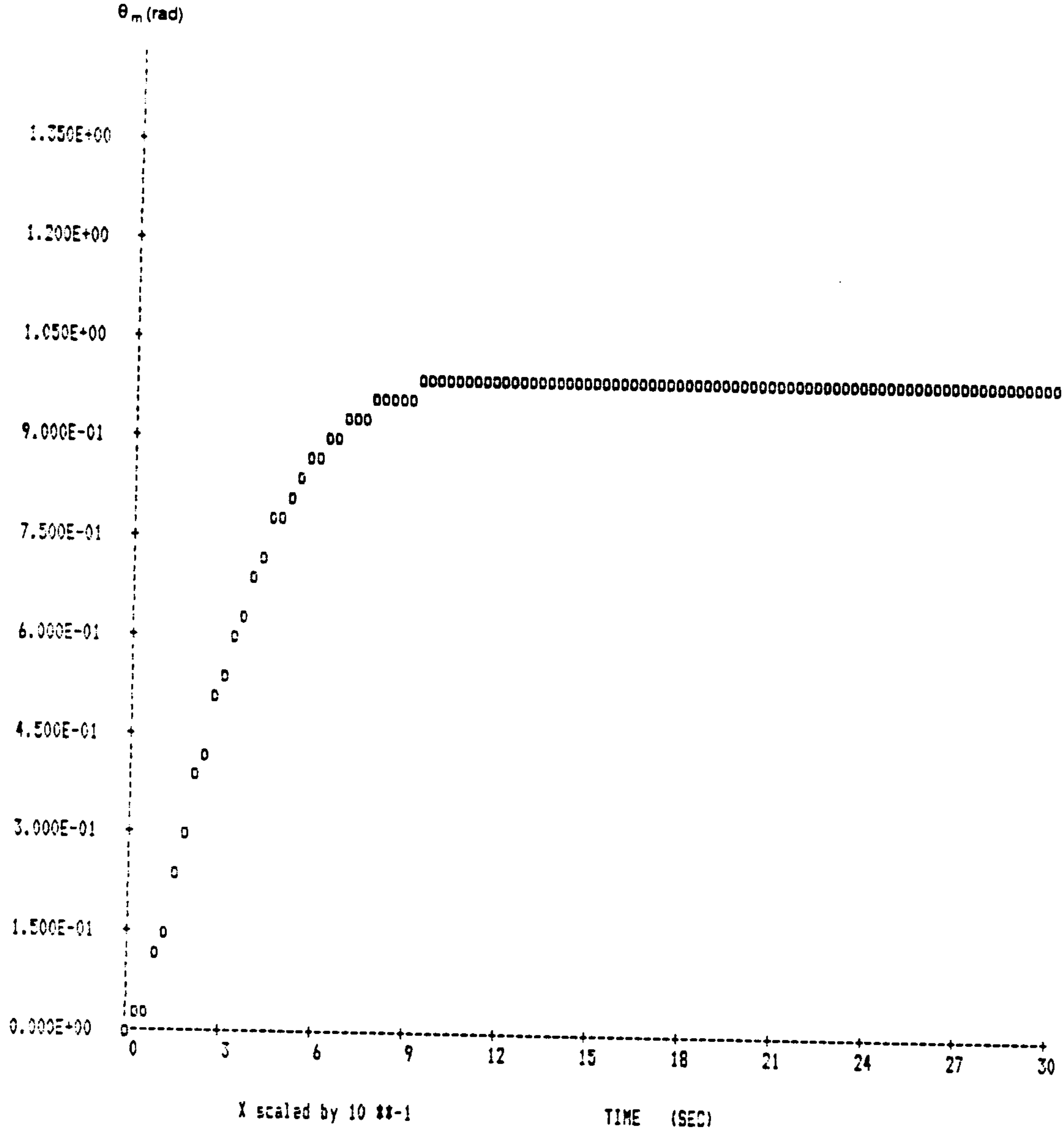

Figure 3.15

Unit-step response of closed-loop uncompensated system output, servomechanism mode

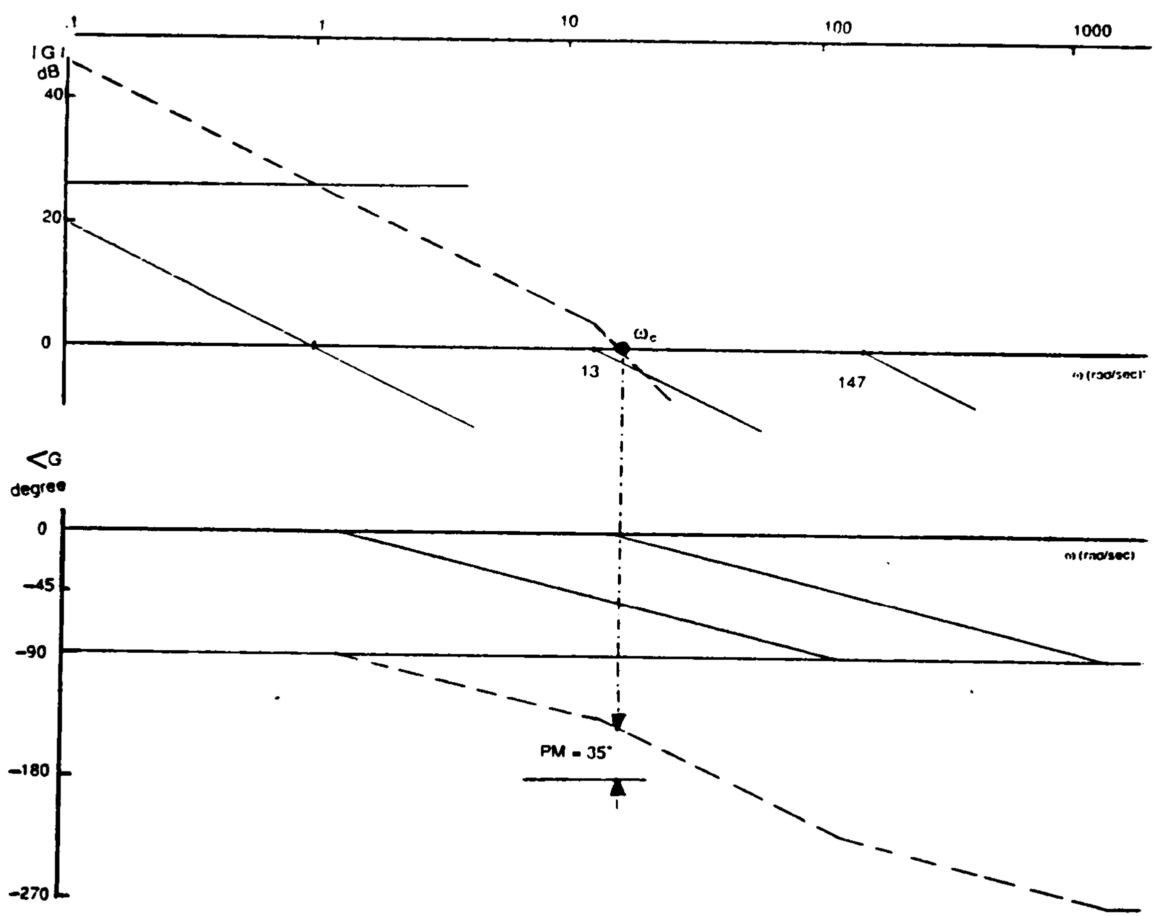

Figure 3.16

Bode plot of adjusted-uncompensated system

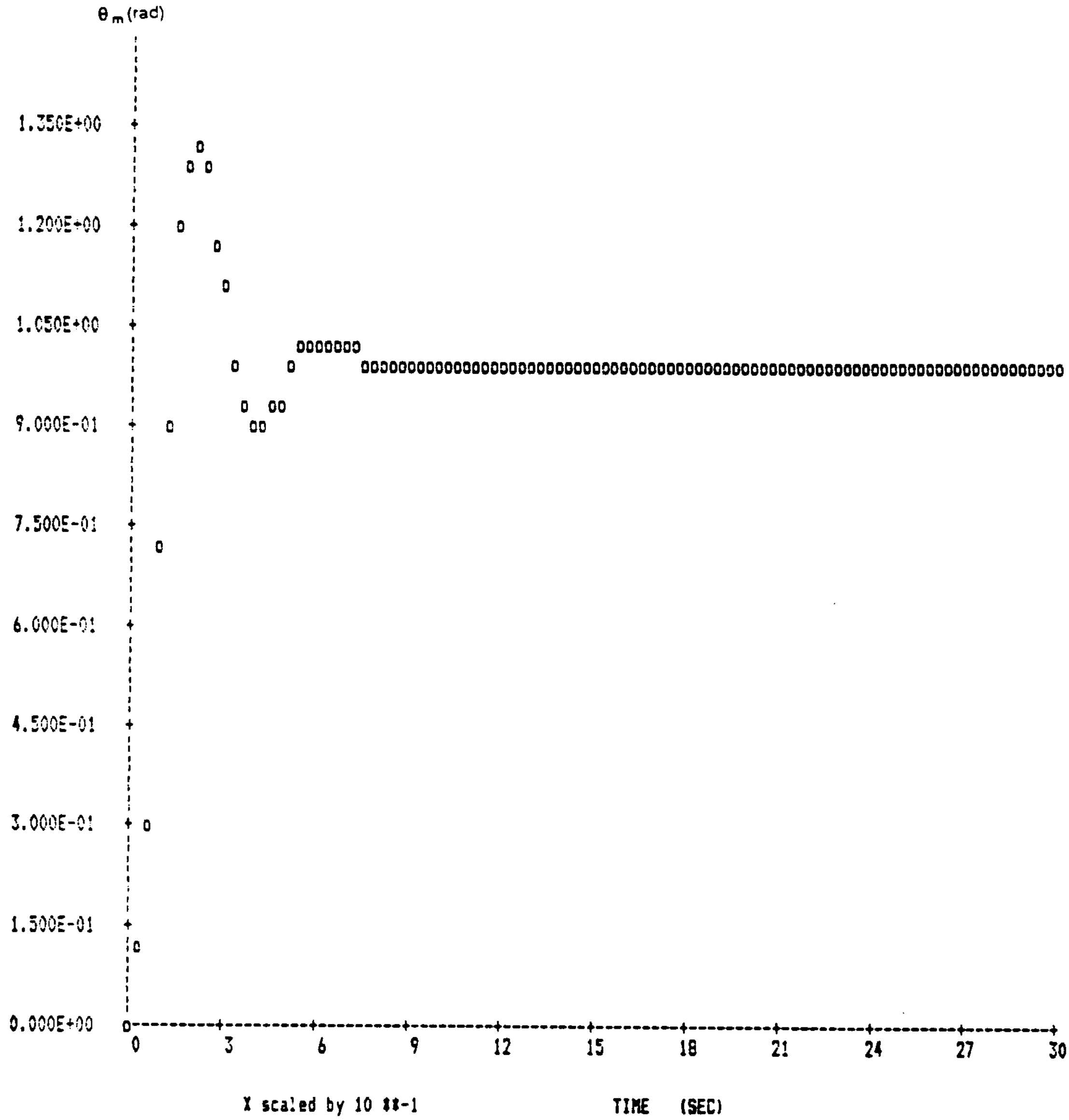

Figure 3.17

Unit-step response of closed-loop adjusted-uncompensated system output, servomechanism mode

where

$K_v = 21$

$PM = 35°$.

In order to lift the phase margin up to 45°, a phase-lag compensator is used, where

$$G_c = \frac{1 + aTS}{1 + TS} = a \cdot \frac{s + \frac{1}{aT}}{s + \frac{1}{T}}, \quad a < 1$$

Designing this compensator, the same steps used before are used here.

First, it is observed from Figure 3.16 that the 45° PM is obtained if the new gain-crossover frequency w'_c is at 10 rad/sec. From the magnitude plot, the value of system gain at $w'_c = 10$ rad/sec is 6 dB. This means that phase-lag compensator must provide an attenuation of 6 dB at this frequency. In order to bring the magnitude curve down to the 0 dB-axis at $w'_c = 10$ rad/sec, the value of a is

$$20 \log_{10} a = -6 \text{ dB}$$

or

$$a = \log_{10}^{-1} - \frac{6}{20} = 0.5$$

The value of "a" indicates the required distance between the two corner frequencies of the phase-lag network so the attenuation of 6 db is realized.

In order that the phase-lag does not appreciably affect the phase curve at the new w'_c, the corner frequency $\frac{1}{aT}$ is chosen to be at one decade below w'_c, so

$$\frac{1}{aT} = \frac{w'_c}{10} = \frac{10}{10} = 1 \text{ rad/sec}.$$

This gives,

$$\frac{1}{T} = a = .5$$

so

$$G_c = a\,\frac{s + \frac{1}{aT}}{s + \frac{1}{T}} = .5\,\frac{s+1}{s+.5} = \frac{1 + \frac{s}{1}}{1 + \frac{s}{.5}}$$

The adjusted, compensated outer-open loop transfer function of the control system is,

$$\frac{\theta_m}{E_a} = \frac{21(1 + \frac{s}{1})}{s(1 + \frac{s}{147})(1 + \frac{s}{13})(1 + \frac{s}{.5})} \tag{3.15}$$

The Bode plot drawn for Equation 3.15 is shown in Figure 3.18 , where $PM = 46°$ and $K_V = 21$.

The unit-step response of the control system is shown on Figure 3.19, where the overshoot is equal to 22% , which is more acceptable, more stable, and more desirable unit-step response for the system than the other two series compensation methods.

Therefore, the inner loop-outer loop compensation controller will be the representative controller for the classical method design, which will be simulated with the wind disturbance input and compared with the simulation of the modern control method.

3.3. Modern Method Design Using LQR

Reasons for picking an optimal controller are that the designer may not really know the desirable closed-loop pole locations, and that choosing pole locations far from the origin may give very fast dynamic response but require control signals that are too large to be produced with the available power source. Use of gains that would be able to produce these signals, in absence of power limitations, could cause the control signals to exceed physical limits. This causes a saturation in the system and a nonlinearity would occur. In such cases the closed-loop dynamic behavior will not be as predicted by the linear analysis, and may be even unstable. To avoid the problems, it is often necessary to limit the speed of response to that which can be achieved without saturation. Another reason for limiting speed of response is a desire to avoid

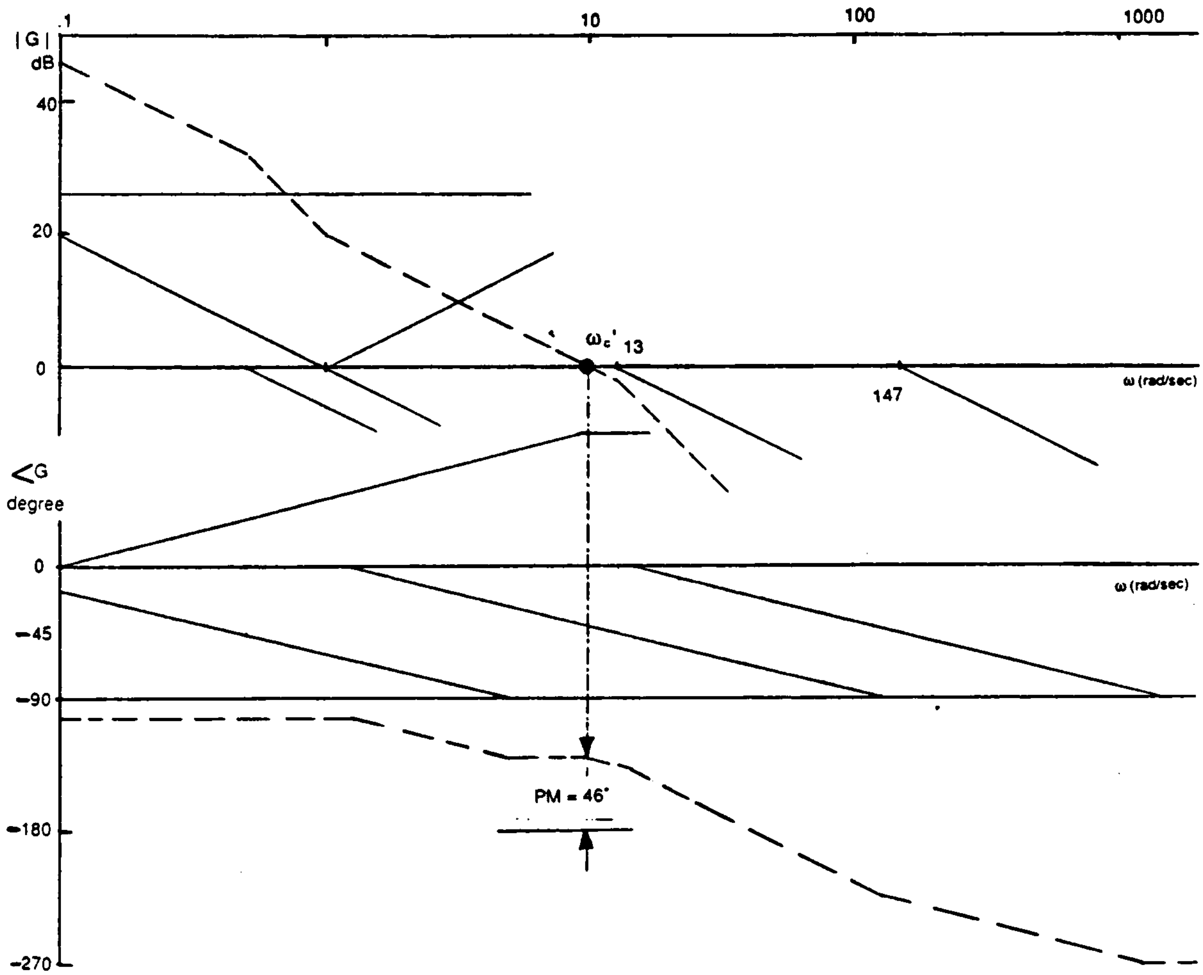

Figure 3.18

Bode plot of compensated system

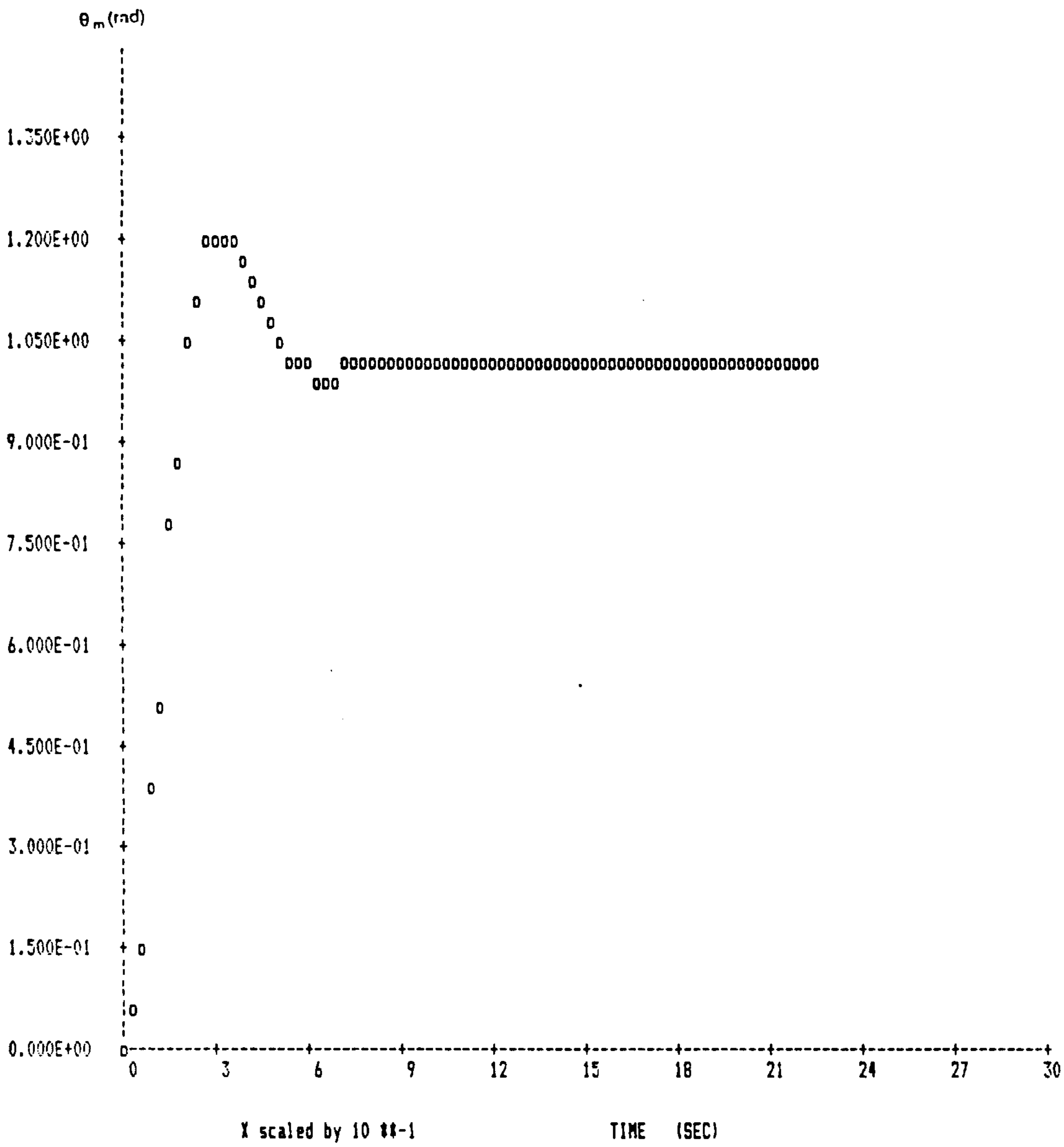

Figure 3.19

Unit-step response of closed-loop compensated system output, servomechanism mode

problems of noise that typically accompany high-gain systems. For a control designer who has an intuitive feel for the proper closed-loop pole locations but is faced with an unfamiliar process to control and a lack of time to acquire the necessary insight, the optimization theory can serve the purpose of providing an initial design while insight is developed. Still another reason for using optimal control theory for design is that the process to be conrolled may not be controllable. This uncontrollable behavior is caused by some subspace of the process state space in which the state vector cannot be moved around by application of suitable control signals. The dynamic behavior in that subspace is not subject to control and hence not all jobs of the closed-loop system can be placed at will. Hence, design by other methods, like pole placement, will not work. But by use of optimum control theory, it is possible to design a control system to control as much as can be controlled. If the behavior of the uncontrollable part is stable, the overall system will behave in an acceptable manner. Also, another good reason for using optimal control is that in a multiple-input or multiple-output system the compensator parameters (gain) are specified, which is not completely the case in using some other methods, especially the pole placement method.

This dynamic process of the system is characterized by the vector-matrix differential equation

$$x^{\bullet} = Ax + Bu \tag{3.16}$$

where

x is the process state variable

u is the control input .

A and B are known matrices of the dynamic system. For the DC motor system, the vector-matrix differential equation or state equation is

$$\begin{bmatrix} di_a(t)/dt \\ dW_m(t)/dt \\ d\theta_m(t)/dt \end{bmatrix} = \begin{bmatrix} \frac{R_a}{L_a} & \frac{-K_b}{L_a} & 0 \\ K_T/J_m & -B_m/J_m & 0 \\ 0 & 1 & 0 \end{bmatrix} \begin{bmatrix} i_a(t) \\ W_m(t) \\ \theta_m(t) \end{bmatrix} + \begin{bmatrix} \frac{1}{L_a} \\ 0 \\ 0 \end{bmatrix} e_a + \begin{bmatrix} 0 \\ \frac{-1}{J_m} \\ 0 \end{bmatrix} T_L$$

and the output equation is

$$y = Cx$$

which is

$$\theta_m(t) = [0 \quad 0 \quad 1] \begin{bmatrix} i_a(t) \\ W_m(t) \\ \theta_m(t) \end{bmatrix}$$

Substituting in the values of the physical parameters found in section 2.5, the above two equations are

$$\begin{bmatrix} di_a(t)/dt \\ dW_m(t)/dt \\ d\theta_m(t)/dt \end{bmatrix} = \begin{bmatrix} -4/25\,10^{-3} & -\dfrac{.65}{25\,10^{-3}} & 0 \\ \dfrac{.65}{6 \times 2.25\,10^{-3}} & \dfrac{-6 \times 1.4\,10^{-3}}{6 \times 2.25\,10^{-3}} & 0 \\ 0 & 1 & 0 \end{bmatrix} \begin{bmatrix} i_a \\ W_m \\ \theta_m \end{bmatrix} + \begin{bmatrix} \dfrac{1}{25\,10^{-3}} \\ 0 \\ 0 \end{bmatrix} e_a + \begin{bmatrix} 0 \\ \dfrac{-1}{6 \times 2.25\,10^{-3}} \\ 0 \end{bmatrix} T_L$$

or

$$\begin{bmatrix} di_a(t)/dt \\ dW_m(t)/dt \\ d\theta_m(t)/dt \end{bmatrix} = \begin{bmatrix} -160 & -26 & 0 \\ 48 & -.62 & 0 \\ 0 & 1 & 0 \end{bmatrix} \begin{bmatrix} i_a \\ W_m \\ \theta_m \end{bmatrix} + \begin{bmatrix} 40 \\ 0 \\ 0 \end{bmatrix} e_a + \begin{bmatrix} 0 \\ -74 \\ 0 \end{bmatrix} T_L \qquad (3.17)$$

and

$$\theta_m(t) = [0 \quad 0 \quad 1] \begin{bmatrix} i_a \\ W_m \\ \theta_m \end{bmatrix} \qquad (3.18)$$

The matrices are represented by

$$A = \begin{bmatrix} -160 & -26 & 0 \\ 48 & -.62 & 0 \\ 0 & 1 & 0 \end{bmatrix}; \quad B = \begin{bmatrix} 40 \\ 0 \\ 0 \end{bmatrix}; \quad B_D = \begin{bmatrix} 0 \\ -74 \\ 0 \end{bmatrix}; \quad C = [0 \quad 0 \quad 1]$$

and $u = e_a$, the system input

T_L = the wind disturbance, considered as a second input . $T_L = 0$ for now.

$$X = \begin{bmatrix} i_a \\ W_m \\ \theta_m \end{bmatrix}$$ is the state variable of the system

$Y = \theta_m$, the system output.

A linear control law is sought.

$$u(t) = -G\,x(t)$$

where G is a suitable gain matrix.

The feedback control system is shown in Figure 3.20. Instead of seeking a gain matrix to achieve specified closed-loop pole locations, a gain is sought to minimize a specified performance criterion V (or cost function) expressed as the integral of a quadratic form in the state x plus a second quadratic form in the control u ;

$$V = \int_t^T [x^T(\tau)\, u(\tau)\, x(\tau) + u^T(\tau)\, Ru(\tau)]d\tau . \qquad (3.19)$$

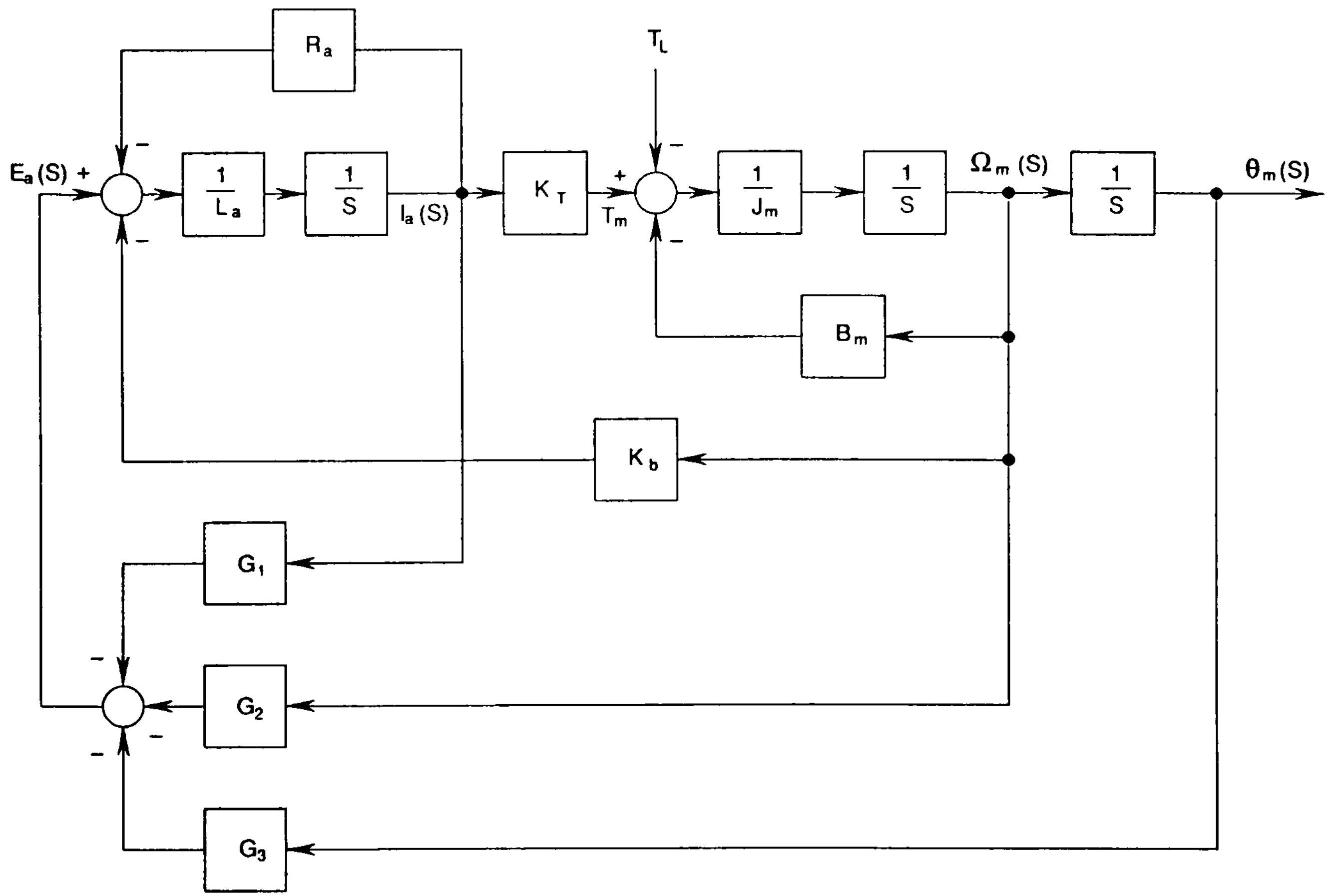

Figure 3.20

Block diagram of linear quadratic regulator

where

> V= the cost function of the quadratic linear regular LQR ;
>
> Q and R are symmetric matrices
>
> t is the present time
>
> T is the final time
>
> $(T - t)$ is the control interval
>
> x^T is the transpose matrix of x

In this case the final time is taken as infinite, so that the optimum control is done by the infinite LQR. The Q and R matrices are called the state weighting matrix and control weighting matrix, respectively. So, the Q and R matrices form some kind of recipe for finding the control gain matrix G along with the known matrices A and B.

The question of concern to the control system designer is the selection of the weighting matrices Q and R in order to minimize the cost function V. In the performance or cost function defined by Equation (3.19) two terms contribute to the integrated cost of control: the quadratic form $x^T Qx$ which represents a penalty on the deviation of the state x from the origin and the term $u^T Ru$ which represents the cost of control.

This means that the desired state is the origin. The weighting matrix Q specifies the importance of the various components of the state vector relative to each other. It should be obvious that the choice of the state weighting matrices depends on what the system designer is trying to achieve. The term $u^T Ru$ is included in an attempt to limit the magnitude of the control signal u. Unless a "cost" is imposed for use of control, a saturation will occur in the control signal. When saturation occurs, the closed loop system behavior, that was predicted on the basis that saturation will not occur, may be very different from the actual system behavior. A system that a linear design predicts to be stable may even be unstable when the control signal is saturated. Thus in a desire to avoid saturation and its consequences, the control signal weighting matrix is selected large enough to avoid saturation of the control signal.

The relationship between the weighting matrices Q and R and the dynamic behavior of the closed-loop system depend of course on the matrices A and B and also are quite complex. A suitable approach for the designer would be to solve for the gain matrices G that result from a range of weighting matrices Q and R, and calculate (or simulate) the corresponding closed-loop response. The gain matrix G that produces the response closest to meeting the design objectives is the ultimate selection. With the use of software like MATLAB which is now widely available, it is easy to solve for G, given A, B, Q, and R. In a few hours time the gain matrices and transient response that result for a large number of combinations of Q and R can be determined, and a suitable selection of G can be made.

When the control law, $u(t) = -Gx(t)$, is used to control the dynamic process of $x^{\bullet} = Ax + Bu$, the closed-loop dynamic behavior is given by Figure 3.21:

$$x^{\bullet} = Ax - BGx + Bu$$

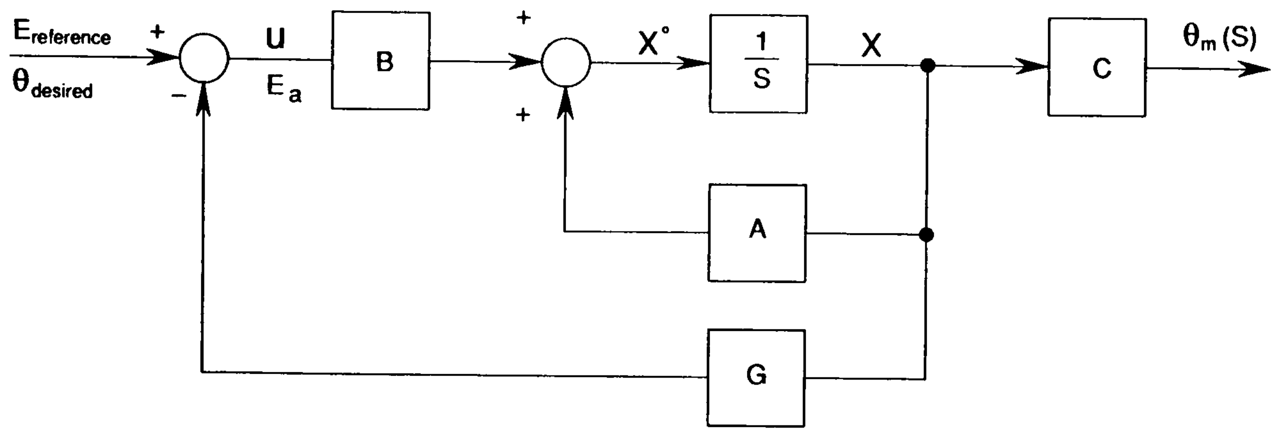

Figure 3.21

State diagram of LQR

$$x^{\bullet} = (A - BG)x + Bu$$

$$x^{\bullet} = A_C\, x + Bu \tag{3.20}$$

where

$$A_C = A - BG\,. \tag{3.21}$$

A_C is the closed-loop dynamix matrix. In general, all matrices A, B, and G are time-varying, but they will be considered later on to be constant. The solution of Equation (3.20) can be written in terms of the general state transition matrix

$$x(\tau) = \phi_C(\tau, t)\; x(t)\,. \tag{3.22}$$

where ϕ_C is the state-transition matrix corresponding to A_C. Using Equation (3.22), the performance index (Equation (3.19)) can be expressed as a quadratic form in the initial state $x(t)$,

$$V = \int_t^T [x^T(\tau)\; Q\; x(\tau) + x^T(\tau)\; G^T\; RG\; x\,(\tau)]d\tau \tag{3.23}$$

$$V = \int_t^T x^T(t)\; \phi_C^T\; c(\tau, t)(Q + G^T\, RG)\phi^c(\tau, t)\; x(t)\; d\tau \tag{3.24}$$

The initial state $x(t)$ can be moved outside the integral to yield

$$V = x^T(t)\, M(t, T)x(t)\,, \tag{3.25}$$

where

$$M(t, T) = \int_t^T \phi_c^T(\tau, t)(Q + G^T RG)\, \phi_c(\tau, t)\, d\tau \tag{3.26}$$

For purposes of determining the optimum gain, the matrix G which results in the closed-loop dynamics matrix $A_c = A - GB$, minimizes the resulting integral in Equation (3.26). It is convenient to find a differential equation satisfied by Equation (3.26). For this purpose, it is noted that V in Equation (3.23) and (3.24) is a function of the initial time t. Thus, Equation (3.23) is written as

$$V(t) = \int_t^T x^T(\tau)\, L(\tau)\, x(\tau)\, d\tau \tag{3.27}$$

where

$$L = Q + G^T RG \tag{3.28}$$

It is noted that L is not restricted to be constant. Thus, by the definition of an integral

$$\frac{dV}{dt} = -x'(\tau)\, Lx(\tau)/_{\tau=t} = -x'(\tau)\, Lx(\tau) \tag{3.29}$$

But, from Equation (3.25),

$$\frac{dV}{dt} = -x^{\bullet T}(\tau)\, M(\tau, T)\, x(t) + x^T(t)\, M^\bullet(t, T)x(t) + x^T(t)\, M(t, T)\, x^\bullet(t) \qquad (3.30)$$

Using the closed-loop differential equation in Equation (3.20), Equation (3.30)

$$\frac{dV}{dt} = x^T(t)[A^T(t)\, M(t, T) + M^\bullet(t, T) + M(t, T)\, Ac(t)]x(t) \qquad (3.31)$$

Comparing Equations (3.31) and (3.29), gives

$$-L = A^T M + M^\bullet + M A_c$$

or

$$-M^\bullet = M A_c + A^T M + L \qquad (3.32)$$

when any gain matrix G is chosen to close the loop, Equation (3.32) is written as

$$-M^\bullet = M(A - BG) + A^T - G^T B^T)M + Q + G^T RG \qquad (3.33)$$

The big task now is to find the matrix G which makes the solution for Equation

(3.33) as small as possible. For any arbitrary initial state $x(t)$ and any matrix G or any matrix $M \neq \hat{M}$,

$$V = x^T \hat{M} x < x^T M x$$

where $\hat{M}$ is the desired smallest solution.

The minimizing matrix $\hat{M}$ that results from the minimizing gain $\hat{G}$ must of course satisfy equation (3.33). So

$$-\hat{M}^{\bullet} = \hat{M}(A - B\hat{G}) + (A^T - \hat{G}^T \hat{B}^T)\hat{M} + Q + \hat{G}^T R\hat{G} \qquad (3.34)$$

Any non-optimum gain matrix G and the corresponding matrix M can be expressed in terms of these matrices:

$$M = \hat{M} + N$$

$$G = \hat{G} + z$$

where

$$-\hat{N}^0 = NA_c + A_c^T N + (\hat{G}^T R - \hat{M}B)z + z^T(R\hat{G} - B^T\hat{M}) + z^T Rz \qquad (3.35)$$

where $A_C = A - BG = A - B(\hat{G} + z)$

Comparing Equations (3.35) and (3.32),

$$L = (\hat{G}^T R - \hat{M}B)z + z^T(R\hat{G} - B^T \hat{M}) + z^T Rz \tag{3.36}$$

Using Equation (3.26),

$$N(t, T) = \int_t^T \phi^T(\tau, t)\, L\, \phi_C(\tau, t)\, d\tau$$

If $\hat{V}$ is minimum, then

$$x^T M x \le x^T(\hat{M} + N)x = x^T\hat{M} x + x^T Nx$$

which implies that the quadratic form $x^T Nx$ must be positive-definite, or at least positive semidefinite.

Looking at L in Equation (3.36), if z is sufficiently small, the linear terms dominate the quadratic term $z^T Rz$. Thus, one can readily find values of z which make L negative-definite, unless the linear term in Equation (3.36) is absent altogether. Thus for the control law G to be optimum,

$$R\hat{G} - B^T \hat{M} = 0 \ .$$

Assuming R matrix is nonsingular,

$$\hat{G} = R^{-1} B^T \hat{M} \tag{3.37}$$

This gives the optimum gain matrix in terms of the solution to the differential equation (3.34) that determines M. When equation (3.37) is substituted into equation (3.34) the following differential equation results for M:

$$-\hat{M}^{\bullet} = \hat{M}A + A^T \hat{M} - \hat{M} BR^{-1} B^T\hat{M} + Q \tag{3.38}$$

Equation (3.38) is known as the Riccati equation which is one of the most famous in the literature of modern control theory. It gives the matrix $\hat{M}$, which, using equation (3.37), gives the optimum gain matrix $\hat{G}$.

For the steady state solution, the control interval is infinite.

$$v_\infty = \int_t^\infty (x^T Qx + u^T Ru)d\tau \tag{3.39}$$

In this case, T is infinite and the integration of equation (3.39) will either converge to a constant matrix $\bar{M}$ or grow without limit. If it converges to a limit, the derivative $\hat{M}^{\bullet}$ tends to zero.

So

$$v_\infty = x^T \bar{M}x$$

where $\bar{M}$ satisfies the algebraic quadratic equation or the Riccati equation

$$0 = \bar{M}A + A^T\bar{M} - \bar{M}BR^{-1}B^T\bar{M} + Q \tag{3.40}$$

and the optimum gain in the steady state is given by

$$\bar{G} = R^{-1}B^T\bar{M} \tag{3.41}$$

For most design applications, the system should be asymptotically stable and the dynamic system defined by (A, B, C) matrices should be controllable and observable.

The system is said to be state controllable if there exists a control G which takes the system from any initial state x_0 to any final state x_f in finite time.

For the system to be state controllable, the controllability matrix Q is of rank n , or the determinant of Q, |Q| is not equal to zero:

$$Q = [B \quad AB \quad A^2B] .$$

$$Q = \begin{bmatrix} 40 & -6400 & 974080 \\ 0 & 1920 & -308360 \\ 0 & 0 & 1920 \end{bmatrix}$$

$|Q| = 1.47.10^8 \neq 0$ and the rank of $Q = n = 3$, where n is the number of state variables. So the system is state controllable.

The system is said to be state observable, every state x (to) can be determined from the knowledge of the system output in finite time $t_1 > t_0$.

For the system to be state observable if the observability matrix R is of rank n, or the determinant of R, $|R|$ is not equal to zero.

$$R = \begin{bmatrix} C \\ CA \\ CA^2 \end{bmatrix} = \begin{bmatrix} 0 & 0 & 1 \\ 0 & 1 & 0 \\ 48 & -.62 & 0 \end{bmatrix}$$

$|R| = 48 \neq 0$ and the rank of $R = n = 3$, so the system is state observable.

The algebraic Riccati equation (ARE) has a unique positive definite solution M which minimizes V_∞ where the control law $U = -R^{-1} B^T Mx$ is used. Setting up the cost function V_∞, different values for Q and R are taken so that we can come up with some suitable values for Q and R in order to satisfy thcat equation for one solution. This solution minimizes the cost function and then optimizes the control system to come up with good tracking and regulator responses for the control system. For choosing

$$Q = \begin{bmatrix} 1 & 0 & 0 \\ 0 & 1 & 0 \\ 0 & 0 & 1 \end{bmatrix} \quad \text{and} \quad R = \rho \, . \, I \text{ where } \rho = \left(\frac{\sigma_{max}}{w_c}\right)^2 .$$

σ_{max} = the maximum singular value of N_S

$N_S = \sqrt{Q} . B$.

Taking $w_C = 40$, the solution for M of the Riccati equation is done by using the MATLAB software. To do that, we create a computer program in MATLAB language in order to give the MATLAB software the needed command statements. Also, the MATLAB will simulate the control system using the two modes of operation separately and will calculate the gain matrix $G = R^{-1} B^T M$. The unit-step response of the LQR control system operating as a servomechanism mode is shown on Figure 3.22 where the tracking response is relatively good.

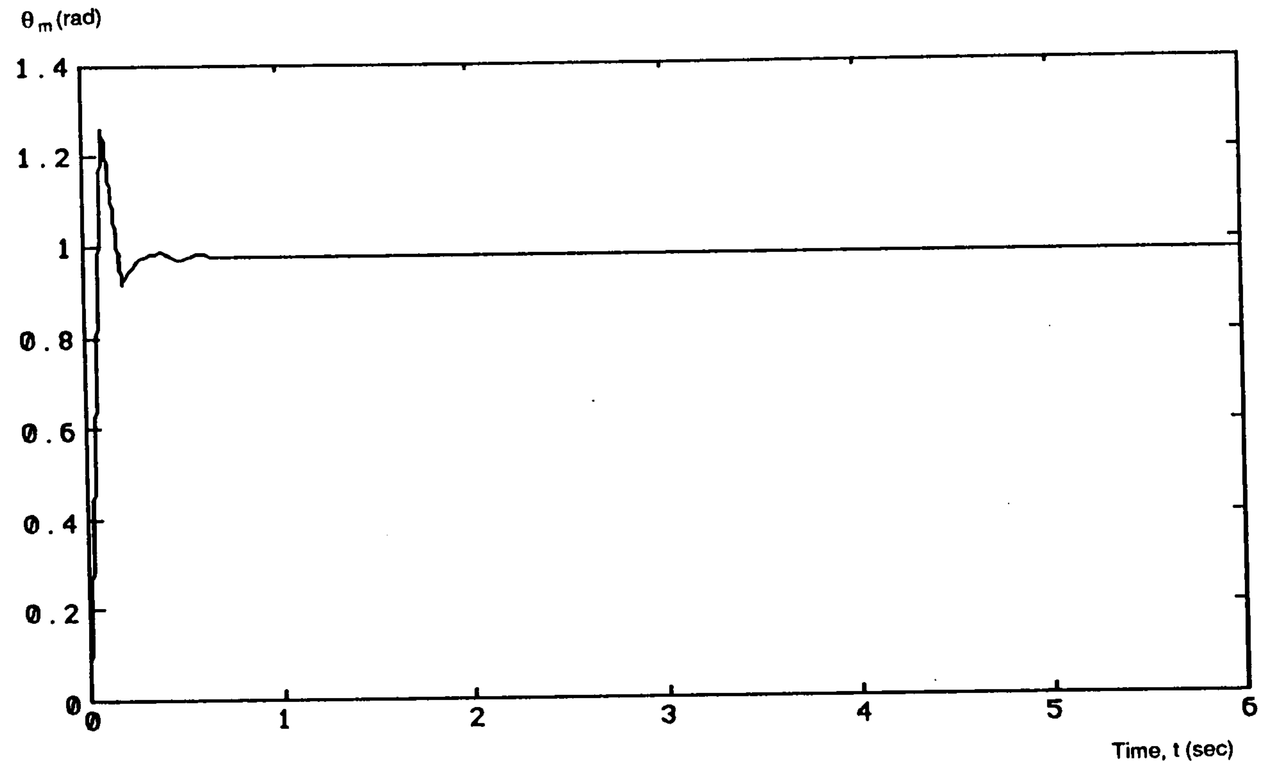

Figure 3.22

Unit-step response of closed-loop compensated system output, using LQR , servomechanism mode

CHAPTER IV

SYSTEM SIMULATION

4.1. Classical Method

The control system transfer function $\frac{\theta_m}{T_L}$, the output angular displacement with respect to the input wind disturbance, is determined taking into account both the inner loop and the outer loop. Since the control system is linear, the effect of the wind disturbance input is taken and analyzed alone without including the original command input, e_a. So, the total response of the control system is the sum of both the command input response, without applying the wind disturbance input, and the wind disturbance input response, without applying the command input. This is permitted by using the superposition theorem of linear control systems. The actual response of the control system is the sum of the servomechanism and regulator modes of operation.

$$\theta_m(t) = \theta_m(e_a) + \theta_m(TL) \tag{4.1}$$

During the analysis and design of the control system, the wind disturbance input was set to zero. After designing both classical and modern controllers for the control system, a simulation is done for the system with the application of torques resulting from wind disturbances. Knowing that the wind disturbance tries to oppose the rotation of the radar antenna and in turn opposes the developed torque and the angular displacement output, the response of the output control system due to the wind gust only behaves negatively. So, the transfer function of $\frac{\theta_m}{T_L}$ is negative.

The simulation of the control system using the classical controller is carried out by deriving the transfer function $\frac{\theta_m}{T_L}$. This is done as follows:

$$\theta_m = \frac{1}{s}\,\Omega_m$$

Using Figure 3.13,

$$\Omega_m = \frac{1}{(J_m s + B_m)} \cdot (T_m - T_L)$$

$$\Omega_m = \frac{K_T}{(J_m s + B_m)(R_a + L_a s)} \{K[(E_a - \theta_m)K_c G_c - .1\,\Omega_m] - K_b \Omega_m\} - \frac{1}{(J_m s + B_m)} T_L$$

For $E_a = 0$ and $\theta_m = \frac{1}{s}\,\Omega_m$,

$$\Omega_m = \frac{K_T}{(J_m s + B_m)(R_a + L_a s)} \{-K K_c G_c \frac{\Omega_m}{s} - .1\,\Omega_m - K_b \Omega_m\} - \frac{1}{(J_m s + B_m)} T_L$$

or

$$\frac{\Omega_m}{T_L} = \frac{-(R_a + L_a s)}{(J_m s + B_m)(R_a + L_a s) + K_T(K K_c G_c \frac{1}{s} + .1K + K_b)}$$

$$\frac{\theta_m}{T_L} = \frac{-(R_a + L_a s)}{s[J_m L_a s^2 + (B_m L_a + J_m R_a)s + B_m R_a + K_T(K K_c G_c \frac{1}{s} + .K + K_b)]}$$

Substituting for the parameter values, K = 3 , and

$$K_c G_c = 7.5 \frac{(1+s)}{(1+2s)}$$

$$\frac{\theta_m}{T_L} = \frac{-74(s+160)(1+2s)}{(s+1)(s+148)(s^2+11.5\,s+139)} \qquad (4.2)$$

The block diagram of Equation 4.2 is shown in Figure 4.1 .

The unit-step response simulation of Equation (4.2) is shown on Figure 4.2, where the output overshoots negatively, and goes back up to settle down approximately at -.2 .

This is relatively accepted for the regulator mode of operation. The closer to zero the steady state output of the system operating as a regulator mode is, the better the automatic tracking system performs.

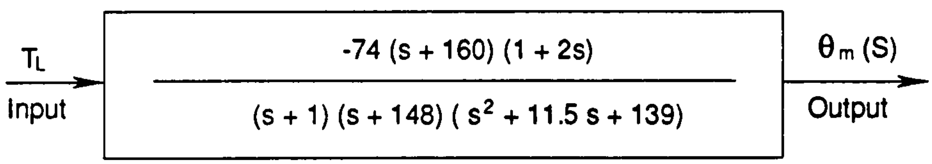

Figure 4.1

Block diagram of transfer function

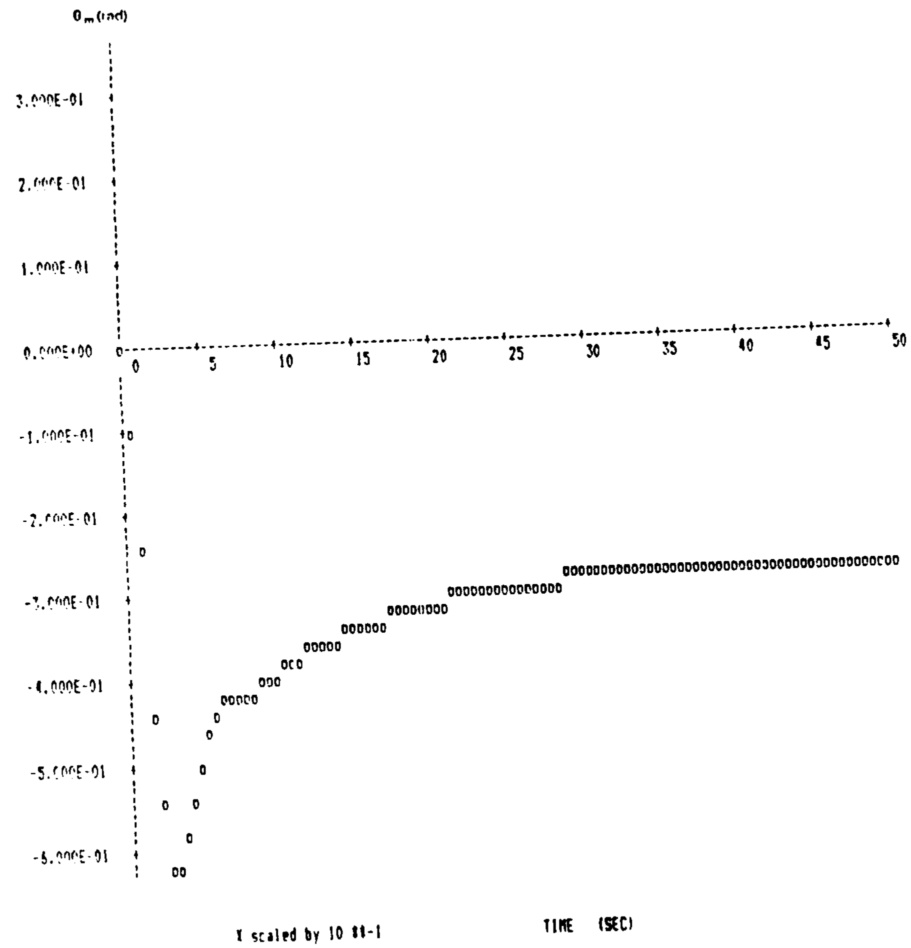

Figure 4.2

Unit-step response of closed-loop compensated system output using inner loop-outer loop, regulator mode

4.2. Modern Method

After the LQR controller is designed for the automatic tracking system in section 3.3, the MATLAB software simulates the LQR control system operating only as a regulator mode, including the disiturbance input dynamic matrix, B_D, and excluding the other input dynamic matrix, B. After the simulation is done, we find that the system output θ_m of the unit-step response goes negatively to -6v and holds there and never goes up to zero regardless of the variation values of Q and R matrices. So, we have a bad regulator mode of operation when the wind disturbance is introduced into the system which has a bad effect in the tracking system performance. So, to deal with this serious problem, a unity feedback is introduced into the system which is fed back from the output θ_m to the voltage input through an amplifier of gain K, as shown in Figure 4.3.

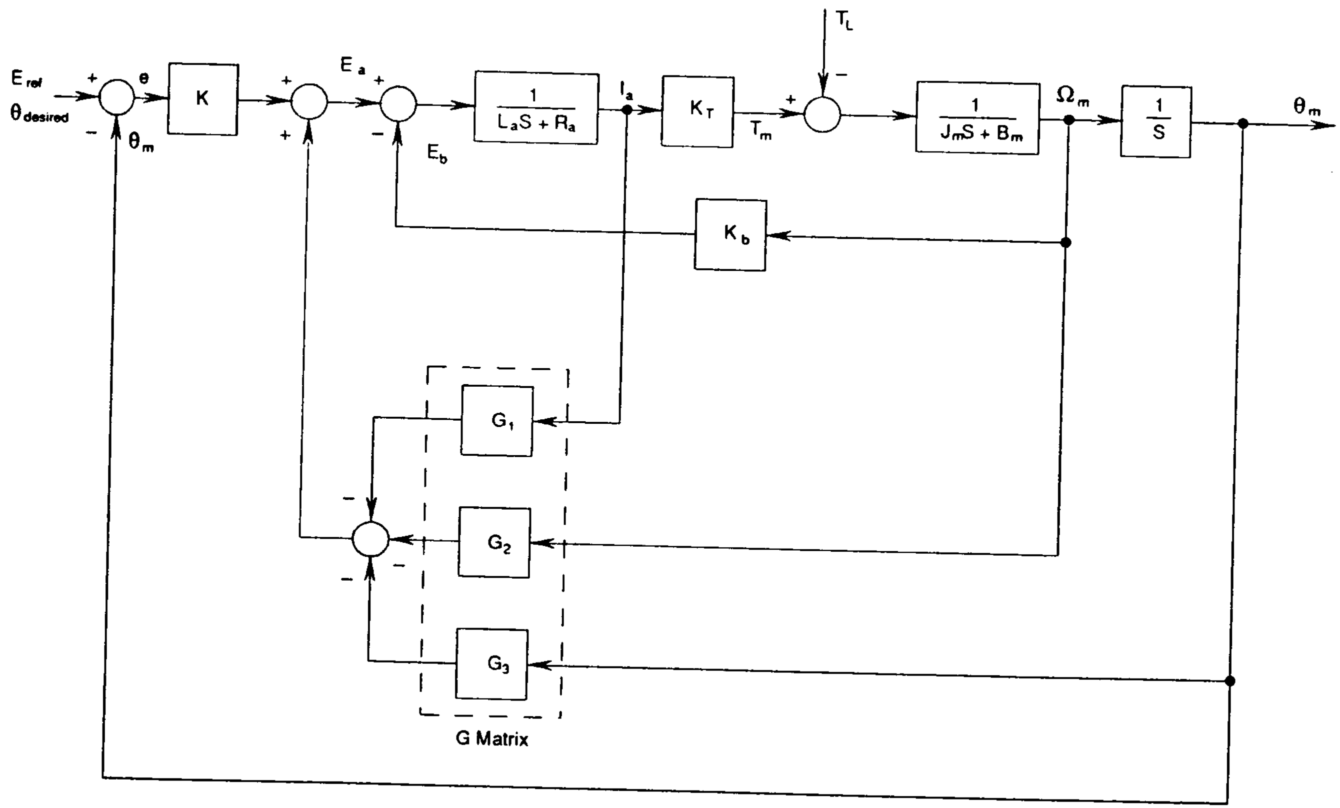

Figure 4.3

Block diagram of linear quadratic regulator, with an output feedback

Letting $\theta = [0 \quad 0 \quad 1]\underline{x}$

$$u = -Gx + K(\theta_d - \theta_m)$$

$$u = -Gx - K[0 \quad 0 \quad 1]x + K\,\theta_d$$

$$x^0 = Ax + Bu + B_D\,T_L$$

$$x^0 = Ax + B(-Gx - K[0 \quad 0 \quad 1]x + K\,\theta_d] + B_D\,T_L$$

$$x0 = (A - BG - KB\,[0 \quad 0 \quad 1])x + KB\,\theta_d + B_D\,T_L\,.$$

The feedback LQR system dynamic equations are:

$$x^0{}_F = A_F\,x + B_F\,\theta_d + B_D\,T_L \tag{4.3}$$

$$\theta_m = Cx \tag{4.4}$$

where $A_F = A - BG - KB[0 \quad 0 \quad 1]$, feedback dynamic matrix,

$B_F = KB$, feedback input matrix

B_D = Disturbance input matrix

θ_d = new reference input

x = state variables (i_a, W_m, θ_m)

A, B = original dynamic matrices of the system

G = control gain matrix of LQR $[G_1 \quad G_2 \quad G_3]$

K = amplifier gain

T_L = wind disturbance.

Calculating $A_F = A - BG - KB\,[0 \quad 0 \quad 1]$,

$$A_F = \begin{bmatrix} (-160 - 40\,G_1) & (-26 - 40\,G_2) & (-40\,G_3 - 40\,K) \\ 48 & -.62 & 0 \\ 0 & 1 & 0 \end{bmatrix}$$

Calculating $B_F = KB$,

$$BF = K \begin{bmatrix} 40 \\ 0 \\ 0 \end{bmatrix} = \begin{bmatrix} 40K \\ 0 \\ 0 \end{bmatrix}$$

$$BD = \begin{bmatrix} 0 \\ -74 \\ 0 \end{bmatrix}$$

$$C = [0 \quad 0 \quad 1]$$

Keeping the same value of Q and taking some different values for w_C and K, the performance of the regulator mode improves considerably. For $w_C = 75$ and $K = 75$, the solution of the Riccati equation M is:

$$M = \begin{bmatrix} .0055 & .0098 & .0133 \\ .0098 & .0419 & .0529 \\ .0133 & .0529 & 1.116 \end{bmatrix}$$

and the calculated gain matrix G is:

$$G = [.78 \quad 1.38 \quad 1.87]$$

The performance of the feedback LQR control system operating as a servomechanism and as a regulator mode is acceptable and good.

Starting with the uncontrol physical system, the unit-step responses of the open-loop uncompensated system state x operating as servomechanism and regulator modes are shown on Figure 4.4 and Figure 4.5 respectively, where the output in both modes goes out of bound.

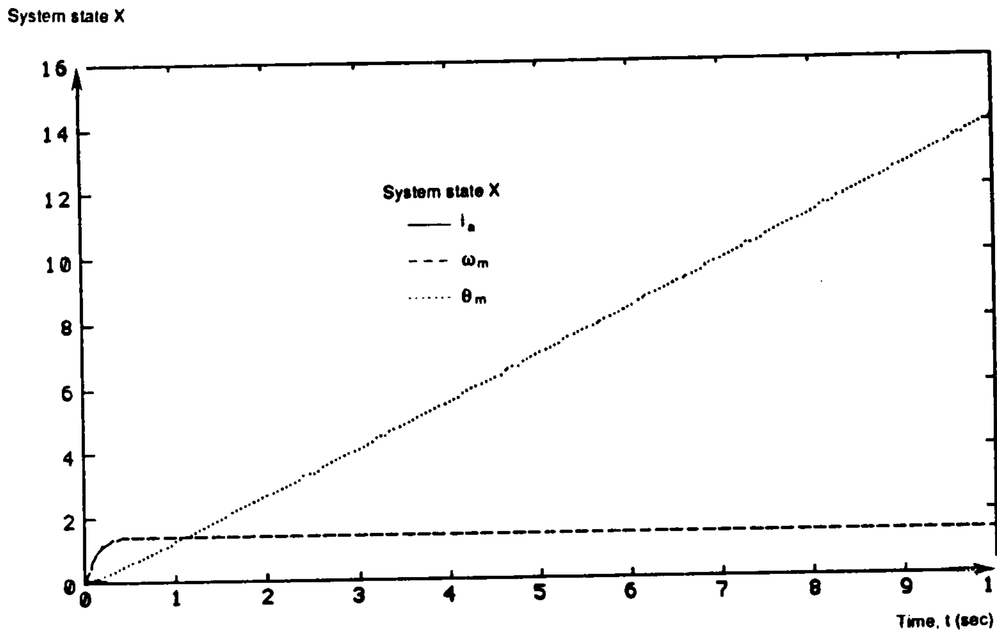

Figure 4.4

Unit-step response of open-loop uncompensated system state X , servomechanism mode

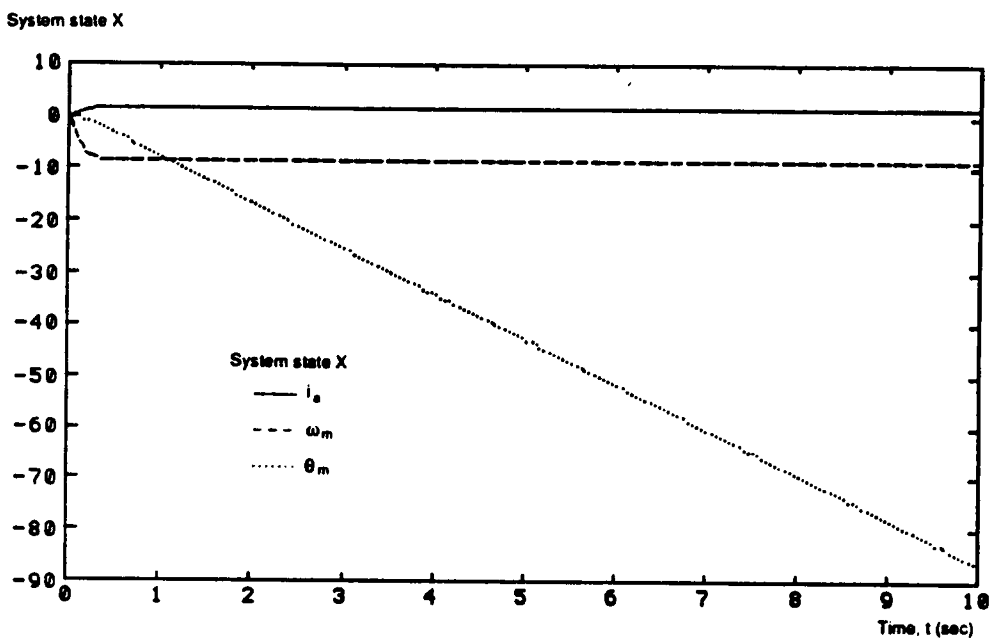

Figure 4.5

Unit-step response of open-loop uncompensated system state X, regulator mode

Also, the unit-step responses of the closed-loop uncompensated system state x operating as servomechanism and regulator modes are shown on Figure 4.6 and Figure 4.7, respectively, where the system output holds at -6v operating as a regulator mode. The unit-step responses of the closed-loop compensated system state x, using LQR-Feedback, operating as servomechanism and regulator modes are shown on Figure 4.8 and Figure 4.9, respectively, where the system output settles down at -.09, very close to zero operating as a regulator mode. In the meantime the output settles nicely at one operating on a servomechanism mode. This is a good performance for the control system operating in both modes, using LQR-feedback controller.

Also, the unit-step responses of the closed-loop compensated system output θ_m, using LQR-Feedback, operating as servomechanism and regulator modes are shown on Figure 4.10 and 4.11, respectively.

The unit-step responses of the closed-loop compensated system output θ_m, using only LQR controller with no feed back, operating as servomechanism and regulator modes are shown on Figure 4.12 and Figure 4.13, respectively, where the output θ_m settles at -6v operating as a regulator mode. This regulator mode of operation is bad and not acceptable. That is why we used the LQR-Feedback controller.

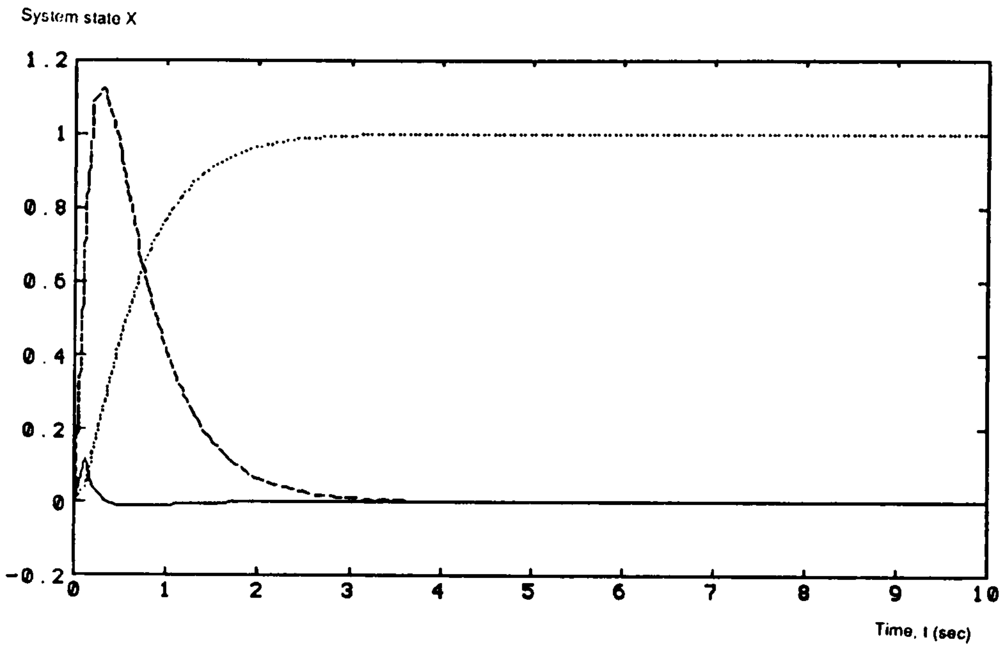

Figure 4.6

Unit-step response of closed-loop uncompensated system state X, servomechanism mode

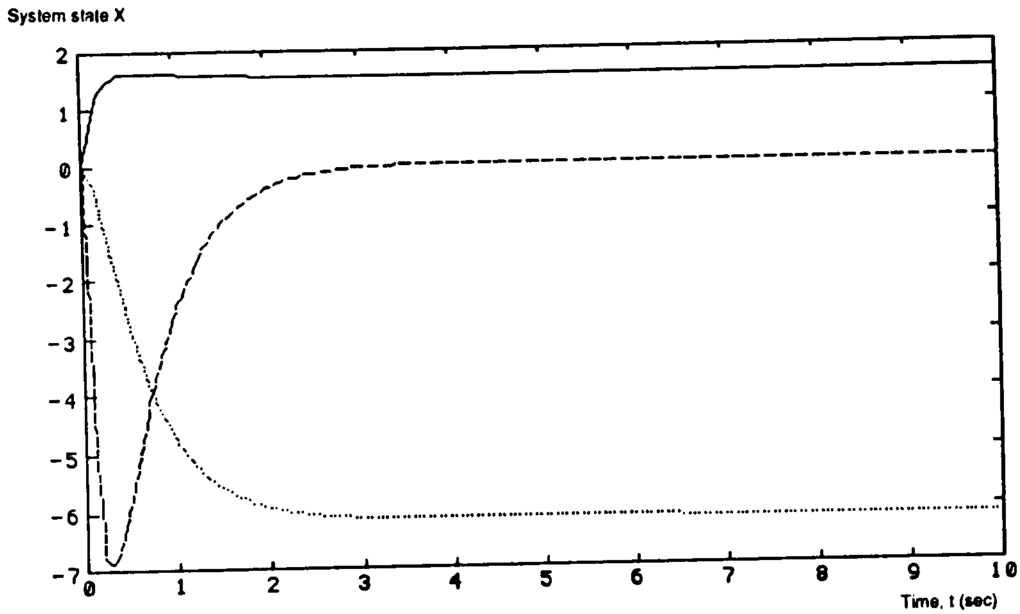

Figure 4.7

Unit-step response of closed-loop uncompensated system state X , regulator mode

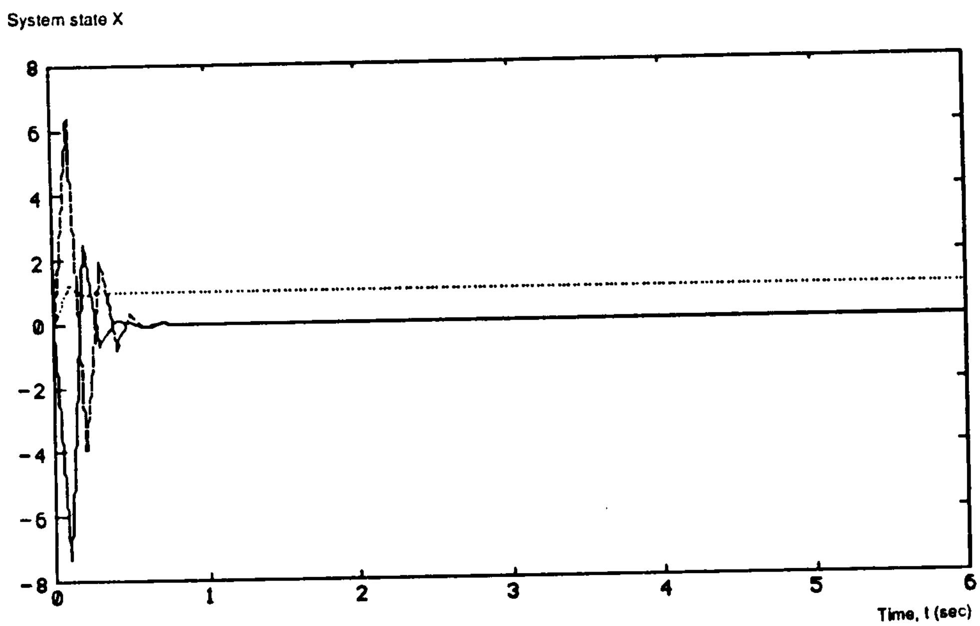

Figure 4.8

Unit-step response of closed-loop compensated system state X using LQR-Feedback, servomechanism mode

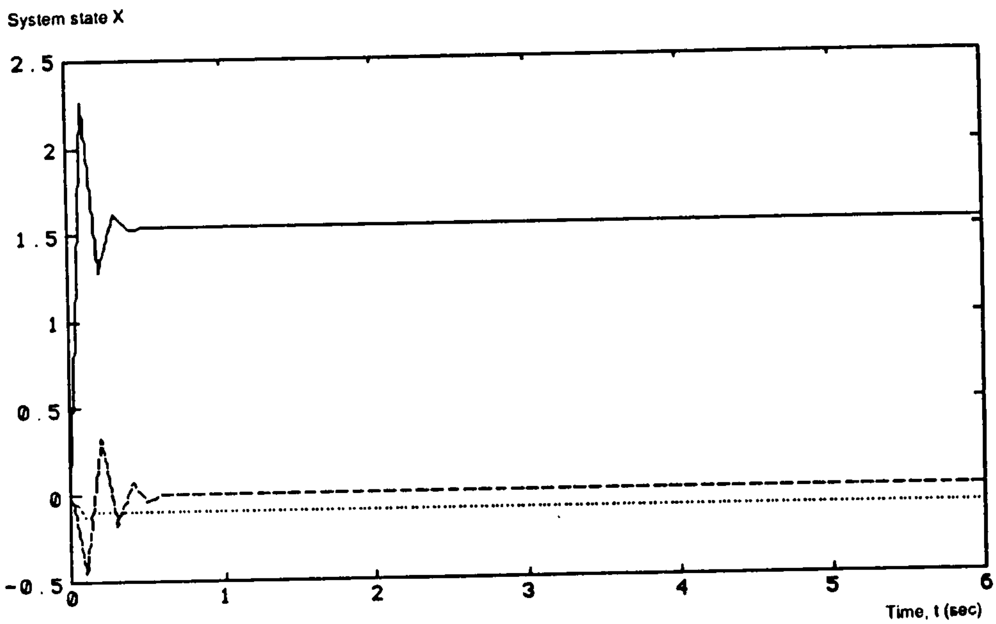

Figure 4.9

Unit-step response of closed-loop compensated system state X using LQR-Feedback, regulator mode

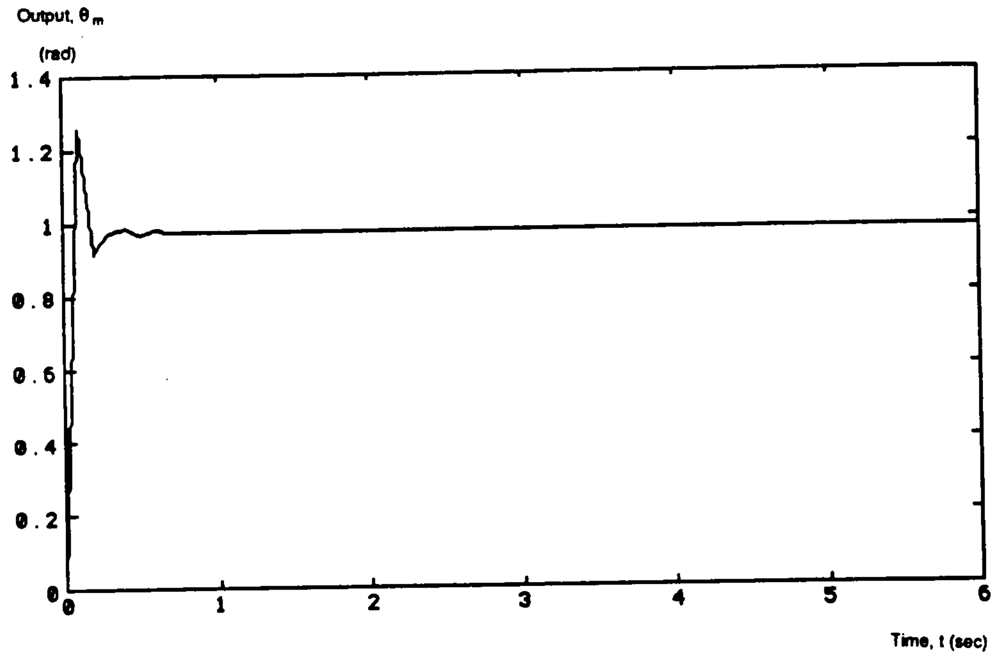

Figure 4.10

Unit-step response of closed-loop compensated system output using LQR-Feedback, servomechanism mode

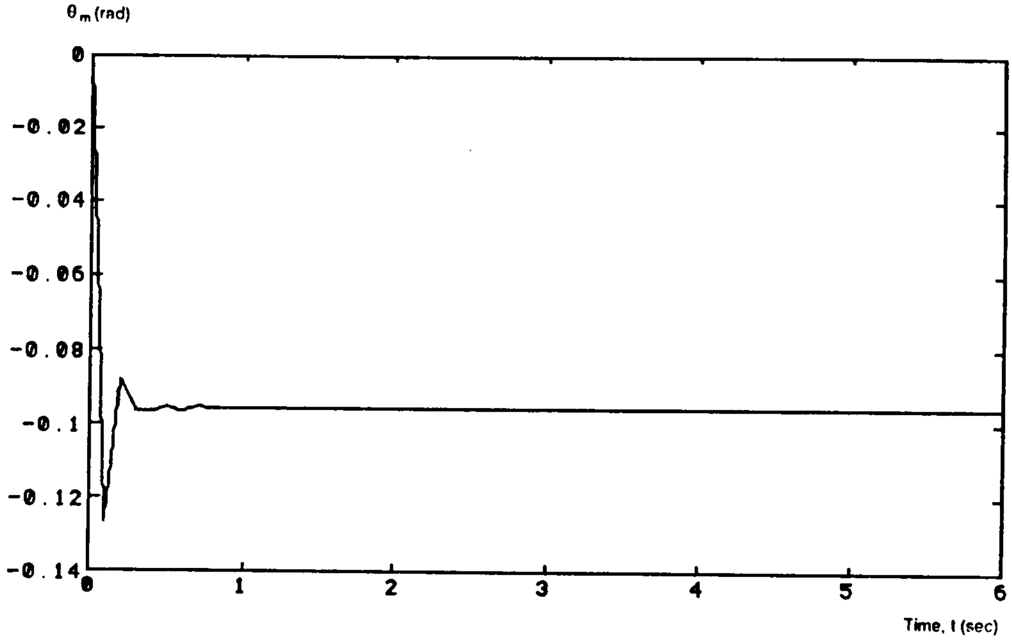

Figure 4.11

Unit-step response of closed-loop compensated system output using LQR-Feedback, regulator mode

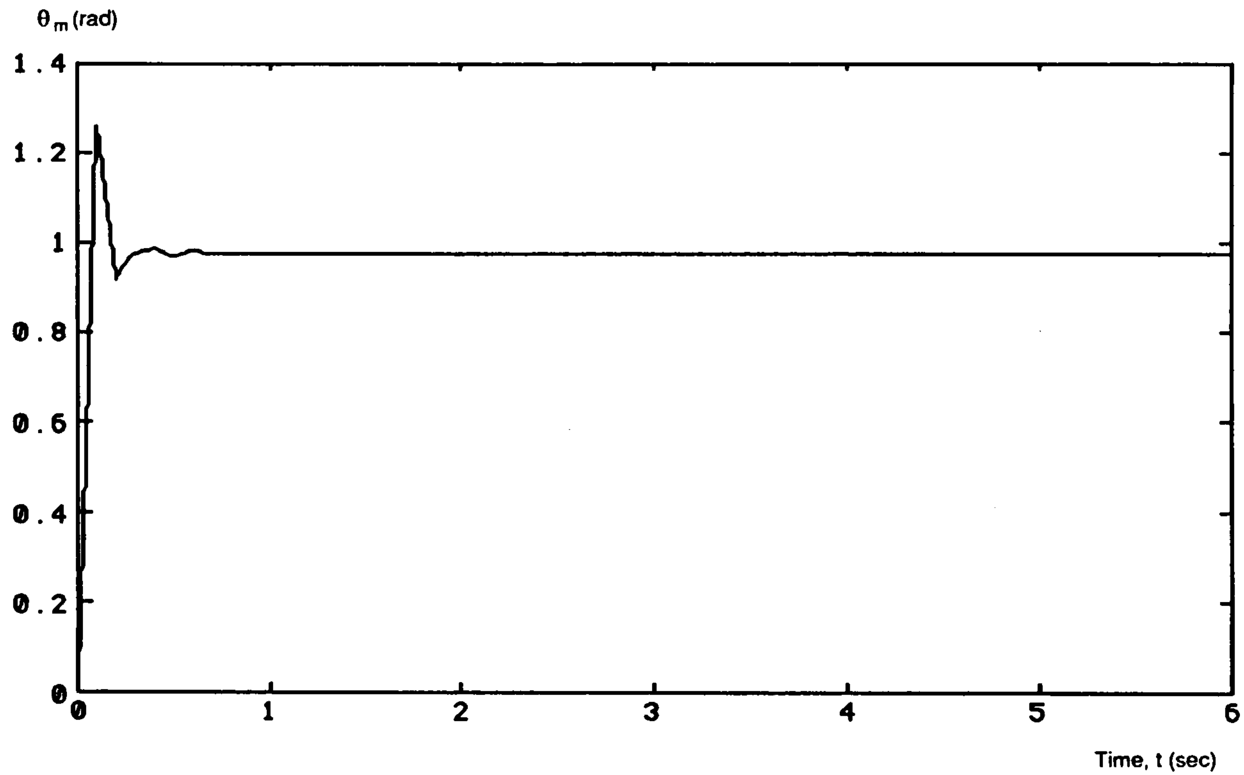

Figure 4.12

Unit-step response of closed-loop compensated system output, using LQR, servomechanism mode

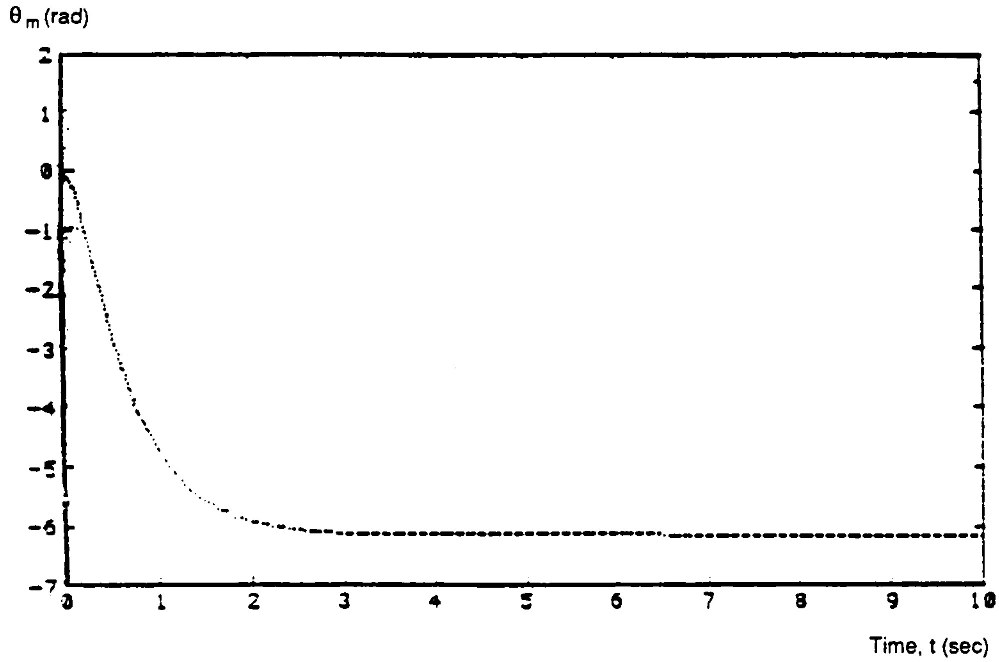

Figure 4.13

Unit-step response of closed-loop compensated output, using LQR, regulator mode

CHAPTER V

CONCLUSION

From the foregoing study of the analysis and design of the control system, we found the following:

1. The inner loop-outer loop classical controller gave the best performance compared to the other two series classical compensators. A phase-lag series compensator was used in the inner loop-outer loop controller, because using a phase-lead would increase the bandwidth and the system becomes noisy. Taking the inner loop-outer loop classical controller as the representative controller for the classical method design, it met all specifications. Operating as a servomechanism mode, the inner loop-outer loop controller gave a good transient response with an acceptable small overshoot, small steady state error and better stability for the system. Operating as a regulator model, the classical controller gave a satisfactory response against the wind disturbance.

2. The modern control approach did not quite meet all the specifications. It gave an acceptable response operating as a servomechanism mode. But operating as a regulator mode, we did not manage to get an acceptable or satisfactory response.

3. The controller using a combination of modern and classical control did the best job, especially when operating as a regulator mode. So, using an LQR controller along with an output feedback, gave the best performance for the

radar antenna drive position control of the automatic tracking system working on both modes of operation, servomechanism and regulator.

One problem we faced in this thesis topic is how to choose the matrices Q and R properly so that the system is optimized and an acceptable performance is resulted for both modes of operation. The solution for this problem is to use the LQR approach as a starting point in the design.

Some additional work can be done for this thesis, like implementing the controllers in a hardware and studying specifically the robustness properties of the control system because the performance characteristics of the transient response do not imply that the system will have good robustness properties. Also, some more studying can be done in order to improve the performance of the system due to the insensitivity to parameter variations and the immunity to noise.

LIST OF REFERENCES

LIST OF REFERENCES

[1] Alexander, J. Eugene and J. Milton Bailey. Systems Engineering Mathematics. Prentice Hall, Inc., Englewood Cliffs, N.J., 1962.

[2] D'Azzo, John J. and Constantine H. Houpis. Linear Control System Analysis and Design. McGraw Hill Book Co., New York, 1981.

[3] Bailey, J. Milton. Class Notes of DC Machines. EE 528, Department of Electrical Engineering, The University of Tennessee, Knoxville, Fall 1989.

[4] Friedland, Bernard. Control System Design. McGraw Hill Book Co., New York, 1986.

[5] Kuo, Benjamin C. Automatic Control Systems. Prentice Hall, Inc., Englewood Cliffs, N.J., 1982.

VITA

My name is Hassan Ahmad Wahab. I was born on August 1, 1963 in Beirut, Lebanon. I grew up in a very loving, dedicated, faithful and poor family. My father could not finish his elementary education because of financial problems due to the poverty and lack of education in south Lebanon at that time. My mother did not even make it to school at all for the same reason. So, my father persisted in giving his children the good education he missed, no matter what it cost him; that is exactly what he did and he was very successful doing that.

I started my elementary education in a public school in BourjalBorajenh, a southern suburb of Beirut, dreaming of becoming an engineer. After three years, I had to transfer with my family to my beautiful, dear hometown, AlRihan, in the south of Lebanon. There, I finished my elementary and secondary education. For business reasons, my family and I had to move back to Beirut. There, I was determined to go to technical high school, although very few students qualify to be admitted to such schools. In 1978 I studied hard and successfully passed the entry examination to be admitted to Amilieh Technical High School.

Because of my fascination with the workings of the television and radio sets I saw, I picked a major in electricity. After the four year program, I explored technically much of the electric world. I graduated from high school in 1982 with high honors. At that time the war in Lebanon, which began in 1975 and continues today, was devistating everything in Beirut, especially when the Israeli Army invaded Lebanon in 1982 and another Holocaust occurred for many groups of people there. To get away from this horrible situation, I decided to leave the country for a chance at a better quality of life and education. First, I decided to go to France because I had been educated in French, but because of a visa problem, I was unable to enter the country. Secondly, I tried to go to Germany, because I had studied German for two years, but this was not possible either. Finally, I tried to come to the U.S.A, the "Land of Opportunity", regardless of my family's bad situation. I was lucky enough to get a visa for the United States and, even more wonderful, I was able to receive financial support from the Horiri Foundation, God bless it. To get this kind of support at the time, you had to be very qualified and have good connections. Thanks to everyone, including my father and my older brother, who helped me receive this support because of its importance in my college success.

I left Lebanon in the spring of 1983 to come to the United States. I attended Tennessee Technological University in Cookeville, Tennessee for one quarter, studying English. After this time, I began my college education. It was a huge challenge for me, leaving my home country and coming into an entirely new culture, but I was able to adapt very quickly. I finished my junior year at Tennessee Tech and transferred to The University of Tennessee, Knoxville. There I finished my B.S. degree in 1987 in Electrical Engineering, and begain persuit of a M.S. degree in Electrical Engineering, with a concentration in power and control.

I now hope to obtain a professional job related to my major, or continue my education, working toward a Ph.D., with God's will.